

# Wade's Rules and the Stability of $\text{Au}_n\text{Ge}_m$ Clusters

Danielle McDermott<sup>1a</sup> and Kathie E. Newman<sup>2b</sup>

<sup>1</sup> Department of Physics, Wabash College, Crawfordsville, IN 47933

<sup>2</sup> Department of Physics, University of Notre Dame, Notre Dame IN 46556

Received: date / Revised version: date

**Abstract.** The properties of clusters formed from two connected  $\text{Ge}_m$  cage-like clusters, such as experimentally synthesized  $\text{Au}_3\text{Ge}_{18}^{5-}$ , are examined using first-principles DFT methods. We focus particularly on  $\text{Au}_n\text{Ge}_{12}^{q-}$  formed from a Wade-rules stable  $\text{Ge}_6$  cluster, where  $n = 0 - 3$  and  $q = 0, 2$ . The geometries, electronic structure, and thermal excitations of these clusters are examined using the SIESTA code. Cluster stability is tested using short molecular dynamics simulations. We find that intercluster bridges between  $\text{Ge}_m$  cages, formed of either Ge-Ge or Au-Ge bonds, can either bind a cluster together or tear it apart depending on the orientation of the bridging atoms with respect to the cages. The properties of neutrally charged  $\text{AuGe}_{12}$  and  $\text{Au}_2\text{Ge}_{12}$  are characterized, and we observe that radially directed molecular orbitals stabilize  $\text{AuGe}_{12}$  while a geometric asymmetry stabilizes  $\text{Au}_2\text{Ge}_{12}$  and  $\text{Au}_3\text{Ge}_{18}$ . A two-dimensional  $^\infty[\text{Au}_2\text{Ge}_6]$  structure is examined and found to be more stable than other periodic  $[\text{Au}_n\text{Ge}_6]$  subunits. While no stable neutral isomers of  $\text{Au}_3\text{Ge}_{12}$  are observed in our calculations, our work suggests additional charge stabilizes isomers of both  $\text{Au}_2\text{Ge}_{12}$  and  $\text{Au}_3\text{Ge}_{12}$ .

**PACS.** 31.15.A 36.40.c 61.46.Bc

## 1 Introduction

The element gold crystallizes in a face-centered cubic (fcc) structure, space group  $Fm\bar{3}m$ , and germanium crystallizes in a diamond structure, space group  $Fd\bar{3}m$ . Gold is a metal, with delocalized electrons, and germanium is a semiconductor, with its bonding electrons localized in covalent bonds. The story of the structure of these elements does not end here. In bulk form, synthetic chemists have grown several exotic crystalline forms of Ge, including a clathrate-II form with the same space group as the familiar semiconductor Ge, but having a 136-atom basis [?,?]. A microcrystalline allotrope of Ge is found, *allo-Ge* [?], by removing Li from a compound  $\text{Li}_7\text{Ge}_{12}$ . *allo-Ge* has a complex orthorhombic structure with 5- and 7-atom rings, space group  $Pmc2_1$ . Upon heating, *allo-Ge* changes form, becoming a hexagonal form of Ge, 4H-Ge, space group  $P6_3mc$ , and then transforming to the standard diamond form,  $\alpha$ -Ge [?]. The thermochemistry of these Ge allotropes have recently been investigated experimentally [?]. Allotropes of Ge are also found by varying pressure, e.g.,  $\beta$ -Ge (space group  $I4_1/amd$ ),  $\gamma$ -Ge or ST12-Ge (space group  $P4_32_12$ ), and  $\delta$ -Ge or BC8-Ge (space group  $Ia\bar{3}$ ) [?,?]. The bonding in these structures is particularly intriguing since in many cases it is not simply the standard  $sp^3$  bonding one finds in group-IV and groups III-V semiconductors.

Gold's story is equally complex, with one interesting aspect being in the evolution of nanostructures of Au with  $N$  atoms to the bulk form. There is evidence that for small values of  $N$ , clusters with icosahedral and other interesting geometric shapes will form [?,?]. Nanoclusters of Au has been often been studied theoretically [?,?,?] and "phase" diagrams of Au as a function of  $N$  have been proposed [?]. Structural phase transition of Au under a variety of stresses have also been studied theoretically [?].

It is known that the elements Au and Ge can combine in bulk form, given another element to provide spacing between groups of Au and Ge atoms. For example, there is a series of  $[\text{AuGe}]$  polyanion compounds where a six-fold ring of alternating Au and Ge forms, and then, dependent on ionic radius of the spacing rare earth ion (Cd, Lu, Sc), the ring is flat, becomes more puckered, and bond angles evolve from ones characteristic of  $sp^2$  bonding to those for  $sp^3$  bonding [?]. In another example, octahedra of  $\text{Au}_5\text{Ge}$  are found in a new compound  $\text{SrAu}_3\text{Ge}$  [?]. Au is often used in catalyzing reactions in Ge, e.g., recently Au was used to self assemble Ge micropatterns on Ge wafers [?]. Fifty years ago, nanoparticles of Au were first used in the Vapor-Liquid-Solid technique to grow nanowires of Si [?]. The growth of Au-catalyzed Ge-nanowires is often studied; it appears that Ge is "fed" from solution or vapor into the Au nanoparticle, with the nanowire being extruded from the base [?]. And while the binary Au-Ge system has a eutectic phase diagram [?], it has been shown that nanowires can be grown below the eutectic temperature [?]. Dayeh

<sup>a</sup> email: mcdermod@wabash.edu

<sup>b</sup> email: newman@nd.edu

*et al.* [?] found Ge nanowire growth to be dependent on the diameter of the wires and related this to the Gibbs-Thomson effect. TEM images show surface melting of the crystalline Au-Ge alloy [?], and more recently, the growth process has been studied using in-situ video rate TEM [?]. Most recently, Gamalski *et al.* [?] observed metastable forms of AuGe during the nanowire growth process. The growth pathways of Ge emerging from Au, as studied recently [?], represent a fascinating challenge for theorists, with some progress being made using semi-empirical models [?,?] and simple kinetic Monte Carlo models of the growth of a “cartoon” nanowire [?]. And from another perspective, almost 25 years ago, it was observed that upon heating, a layer of Au grown on amorphous Ge would pass through the material, crystallizing it [?]. It appears that an atomic-scale description of Au-Ge bonds is essential for a broader physical understanding of these kinetic processes. We find the nanowire problem to be particularly fascinating, but unless one works with phenomenological or nearly phenomenological models of bonding, one cannot hope to study the numbers of atoms that must be involved in the process of nucleating nanowire growth.

Our approach is to study the electronic structure of small clusters of Ge or Ge combined with Au. The tool that we utilize in our study is a first principles density functional theory (DFT) implemented with the SIESTA (Spanish Initiative for Electronic Simulations with Thousands of Atoms) code [?,?]. This allows us to investigate at an electronic level how a gold environment will effect the bonding of germanium in a cluster. A goal is to find stabilizing trends and thus identify possible building blocks for new compounds of Au with Ge. We investigate in particular cages of six or nine Ge atoms, including how they link together with and without the presence of Au atoms.

Ge clusters have previously been studied theoretically as a function of number (e.g.,  $n = 5 - 10$  [?],  $n = 1 - 6$  [?],  $n = 12 - 29$  [?],  $n = 40 - 44$  [?] and, for smaller clusters, as a function of charge [?, ?, ?, ?, ?]. Techniques used typically include DFT. As the number  $n$  increases, studies focus on interesting “motifs,” e.g., plate-like [?] and structures that are building blocks for larger clusters [?], and because of large size, are searched for with genetic algorithms. Experimental gas-phase cluster studies show an evolution from prolate to more spherical geometries occurring at  $n \approx 40$  [?]. Au-Ge nanoparticles have been recently fabricated using laser ablation in water [?], finding clusters with a chainlike morphology. Recently, Li *et al.* [?,?] have studied Au-doped  $\text{Ge}_n$  clusters with  $n = 1 - 13$ , confirming that small gas phase Au-Ge clusters are amorphous, as observed experimentally [?]. More recently, theorists have focused on endohedral Ge clusters encapsulating a metal ion [?,?].

Interestingly, experimentalists have formed anionic clusters  $\text{AuGe}_{18}$  [?],  $\text{Au}_3\text{Ge}_{18}^{5-}$  [?], and  $\text{Au}_3\text{Ge}_{45}^{9-}$  [?]; all have a building block  $\text{Ge}_9^{3-}$ . As studied in Zintl ion chemistry, these building blocks are found in solids such as  $\text{Cs}_4\text{Ge}_9$  [?]. These same building blocks provide a method of synthesizing crystalline and micro-crystalline Ge solids [?,?] and the clathrate-II phase  $\text{Ge}_{136}$  [?]. *allo*-Ge[?] is another

Zintl-ion example, formed by removing Li from a Zintl compound  $\text{Li}_7\text{Ge}_{12}$ . Ge Zintl ions are stabilized by delocalized electrons, follow Wade’s Rules (also known as Wade-Mingos’ Rules) [?, ?, ?], and reveal bonding environments beyond the  $\text{sp}^3$  bonds of bulk Ge structures [?]. This is the starting point of our study.

Wade studied the element Boron, trying to understand its molecular structure as a function of charge state and observed molecular clusters that formed in polyhedral shapes, either as a complete polyhedron or one missing one or more vertices. The number of vertices was counted by Wade as  $n - 1$ , with  $n + 1$  being related to the number of skeletal electron pairs (SEPs). Closed polyhedra were referred to as *closo*. One missing a single vertex was termed “nestlike,” *nido*, and one missing two vertices was “spider-like,” *arachno*. Often, Wade’s rules are rewritten, with the number of vertices now becoming  $n$  so that *closo*, *nido*, and *arachno* clusters have  $(n + 1)$ ,  $(n + 2)$ , and  $(n + 3)$  SEPs, respectively. The deltahedral cages with 5 to 12 vertices are termed “trigonal bipyramid” (5), “octahedron” (6), “pentagonal bipyramid” (7), “dodecahedron” (8), “truncated trigonal prism” (9), “bicapped square-antiprism” (10), “octadecahedron” (11), and “icosahedron” (12). Note that  $\text{B}_6\text{H}_6^{2-}$  is structurally and orbitally similar to  $\text{Ge}_6^{2-}$ , and should have octahedral,  $O_h$  symmetry. Counting available electrons in  $\text{B}_6\text{H}_6^{2-}$ , each B provides 3 and each H provides 1, so the total is  $26 = 6 \times 4 + 2$ . The six covalent B-H bonds use up 12 electrons, leaving 14 electrons for 12 B-B bonds. Traditional two-center two-electron (2c2e) bonds cannot stabilize this structure. The electrons are thus delocalized. Counting the skeletal electron pairs,  $14/2 = 7$ , so a *closo* octahedron can be formed with Wade’s Rules.

In this paper, we focus our work on  $\text{Ge}_m^{q-}$  clusters, where  $m = 6, 9, 12$ , with emphasis on the less studied  $\text{Ge}_6$  cage geometry. We examine the stability of these cages when a bridge of one to three Au atoms is used to connect two nominally identical  $\text{Ge}_m^{q-}$  clusters. The SIESTA techniques used include Conjugate Gradient (CG) minimization, study of the electronic properties using densities of states and an electronic partitioning method, visualization of the molecular orbitals, Crystal Overlap Hamiltonian Population (COHP) [?], and molecular dynamics (MD).

## 2 Methods

We have carried out electronic structure calculations with the fully *ab initio* DFT code SIESTA [?,?] which uses Troullier-Martins norm-conserving pseudopotentials [?] in the Kleinman-Bylander form [?]. The Kohn-Sham [?] wave function was expanded with basis sets of the localized atomic orbitals (LCAO) of the method by Sankey and Niklewski [?]. The localization is a key advantage in studying charged states in molecular or nanosized systems. We use double-zeta polarized (DZP) orbitals and the Generalized Gradient Approximation (GGA) of Perdew, Burke, and Ernzerhof [?] for the exchange-correlation energy functional.

The Ge basis set has cutoff radii for the 4s orbital of 7.12, 1.92 Bohr; 4p of 7.72, 4.92 Bohr; and a polarization

orbital  $4d$  with a cutoff of 7.79 Bohr [?]. The Au basis set has cutoff radii of  $5d$ : 7.20, 5.57 Bohr;  $6s$ : 6.50, 5.50 Bohr; and a polarization orbital  $6p$ : 5.85 Bohr. Soft-confinement potentials and an ionic core are used to create basis orbitals [?]. The Au pseudopotential includes the semicore  $5d^{10}$  states [?, ?, ?]. Both Au and Ge use a partial-core correction to treat overlap between valence and core electrons.

The charge density is represented on a real-space grid with an energy cutoff of 100 Ry. A Monkhorst-Pack  $k$ -point mesh of  $10 \times 10 \times 10$  ensured convergence. We used a Conjugate Gradient (CG) minimization with a maximum force tolerance of  $0.04 \text{ eV/\AA}$  to reveal the local coordinate relaxations. For our molecular dynamics (MD) runs, we use the Nosé thermostat [?] to simulate the canonical ensemble (NVT) with a Nosé mass of  $200 \text{ Ry fs}^2$ . We test the stability of our systems by subjecting them to a temperature of 600K during 1000 steps, each of 2 fs, as suggested by Ref. [?].

The COHP uses DFT matrix elements to separate electronic bonding states from antibonding states in the DOS. In both the DOS and COHP curves we use a small smearing value,  $s \approx 0.1$ , and a high number of sampling points,  $n \approx 500$ , to create smooth electronic structure curves. We treat neighbor interactions within  $0.4 \text{ \AA}$  of the maximal considered “bond” lengths [?]. In examining the electronic states, we focus on the hybridization of the levels presented as indicators of electron delocalization.

## 3 Results

### 3.1 $\text{Ge}_6$ and $\text{Ge}_9$ Clusters

Ge is an example of a main-group element that participates in delocalized cage bonding.  $\text{Ge}_6$  cages have been experimentally synthesized in gas phase [?] and solids [?, ?]. Richards *et al.* isolated the octahedral  $\text{Ge}_6$  cluster, stabilized by organic groups, with reductive coupling [?].  $\text{Ge}_6$  cages have been studied computationally [?, ?] with a focus on the effects of ionic charge on cluster geometry: neutral  $\text{Ge}_6$  flattens to a  $C_{2v}$  symmetry while ionic  $\text{Ge}_6^{2-}$  has octahedral  $O_h$  symmetry, as predicted by Wade’s Rules. The neutral  $\text{Ge}_6$  geometry was also observed by Zhao *et al.* [?] in a computational study which focused primarily on fragmentation behavior in  $\text{Ge}_n$  clusters, and indicates  $\text{Ge}_6$  as a common fragment of larger clusters. Tantalizingly, two types of chains of  $\text{Ge}_9$  have been studied experimentally,  $(-\text{Ge}_9^{2-})_\infty$  [?, ?] and a trimer having the form  $[\text{Ge}_9=\text{Ge}_9=\text{Ge}_9]^{6-}$  [?]. Theorists have analyzed the localized bonds in these chains [?] and examined nanoclusters based on  $\text{Ge}_9$  clusters [?].

Using CG minimization in SIESTA, we initialize the geometries of  $\text{Ge}_6$  and  $[\text{Ge}_6]^{2-}$  clusters as octahedra with atomic coordinates  $\pm(a, 0, 0)$ ,  $\pm(0, a, 0)$ ,  $\pm(0, 0, a)$  using  $a \approx 2.12 \text{ \AA}$ , or initial Ge-Ge separations of  $3.0 \text{ \AA}$ . Our relaxed clusters have the same geometries as King *et al.* [?]. Calculating a minimum and maximum relaxed Ge-Ge distance in  $\text{Ge}_6$ , we find respectively  $2.53 \text{ \AA}$  and  $2.85 \text{ \AA}$ , compared with previous calculations of  $2.58 \text{ \AA}$  and  $2.81 \text{ \AA}$  [?

and  $2.47 \text{ \AA}$  and  $2.85 \text{ \AA}$  [?]. Our calculated bond length,  $2.68 \text{ \AA}$ , for octahedral  $[\text{Ge}_6]^{2-}$  compares favorably with that of  $2.69 \text{ \AA}$  from Ref. [?], and has been measured to be  $2.63 \text{ \AA}$  [?] in a ligand stabilized system.

Our calculated total density of states (DOS) and partial density of states (pDOS) of (a)  $\text{Ge}_6$  and (b)  $\text{Ge}_6^{2-}$  are shown in Fig. 1. The pDOS shows orbitals dominated by  $4s$  character below  $E - E_F = -2.0 \text{ eV}$  and by  $4p$  in the range  $-2.0 \text{ eV} < E - E_F < 0.0 \text{ eV}$ . In the neutral  $\text{Ge}_6$  cluster, we see a stronger hybridization of atomic states, as shown in Fig. 1(a) when compared with (b)  $[\text{Ge}_6]^{2-}$ . This is further confirmed by the MOs, shown in Fig. 2 along with the corresponding energy levels (within  $\pm 0.1 \text{ eV}$ ). Our calculated MO energy levels for  $\text{Ge}_6$  and  $[\text{Ge}_6]^{2-}$  compare favorably to the results found by King *et al.* [?]. The overall symmetries and degeneracies match Table 5 in Ref. [?], however, due to different basis sets, we find a consistent energy shift of approximately 2-3 eV for  $[\text{Ge}_6]^{2-}$  and 5.5-6.5 eV for  $\text{Ge}_6$ . The two additional electrons in  $[\text{Ge}_6]^{2-}$  shift the Fermi energy,  $E_F$ , upward and allow a thirteenth orbital to be occupied. This presumably drives the symmetry change to  $O_h$ , with  $p$  electrons now able to reside in a cubic environment.

We characterize cluster symmetry with a measure of deviation,  $\sigma_{d_G}$ , of the cluster from a perfect octahedron. We average over the twelve skeletal Ge-Ge distances of a single cluster, calculate the standard deviation  $\sigma_{d_G}$  of this value, and report  $\bar{d}_G \pm \sigma_{d_G}$ . A perfect octahedral cluster is composed of twelve identical bonds with  $\sigma_{d_G} = 0.0 \text{ \AA}$ . Some deformation from  $O_h$  symmetry may occur even while  $\sigma_{d_G}$  remains zero; for instance we observe  $\text{Ge}_6^{2-}$  has nearly identical bondlengths of  $\bar{d}_G = 2.68 \text{ \AA}$  such that  $\sigma_{d_G} = 0.0 \text{ \AA}$  yet it is slightly flattened. The neutral  $\text{Ge}_6$  cluster with  $C_{2v}$  symmetry yields  $\bar{d}_G = 2.68 \pm 0.20 \text{ \AA}$ , the agreement of the average bondlength is coincidental since the neutral cluster is composed of eight short bonds  $d \approx 2.5 \text{ \AA}$  and four long bonds  $d \approx 2.8 \text{ \AA}$ .

For  $\text{Ge}_9$ , we initialize the CG relaxation using previously reported geometries and observe very similar clusters to those previously calculated in Refs. [?, ?, ?, ?] both in geometry and electronic structure. Consistent with Wade’s rules, we observe the symmetry of  $\text{Ge}_9^{q-}$  increases to  $D_{3v}$  with  $q = 2$  and  $C_{4h}$  with  $q = 4$  as in Ref. [?]. We see a qualitative agreement in the MOs, with the same symmetries and approximate energies levels as previously reported.

Binding energies  $E_B$  and Fermi gaps  $E_{\text{gap}}$  are shown in Table 1 for the  $\text{Ge}_m$  clusters.  $E_B$  is calculated through out this paper as:

$$E_B = \frac{E_T - (N_A E_A + N_G E_G)}{N_A + N_G} \quad (1)$$

where  $N_A$  and  $N_G$  are the total number of Au and Ge atoms, and  $E_T$ ,  $E_A$ , and  $E_G$  are the SIESTA calculated total energies for the cluster and isolated atoms, respectively. Our calculation shows systematically higher  $E_B$ , than previously reported for pure Ge clusters. The systematic difference in  $E_B$  is consistent with cohesive energies calculated with SIESTA in Ref. [?] for bulk Si and elsewhere. While our values of  $E_{\text{gap}}$  differ, given slight

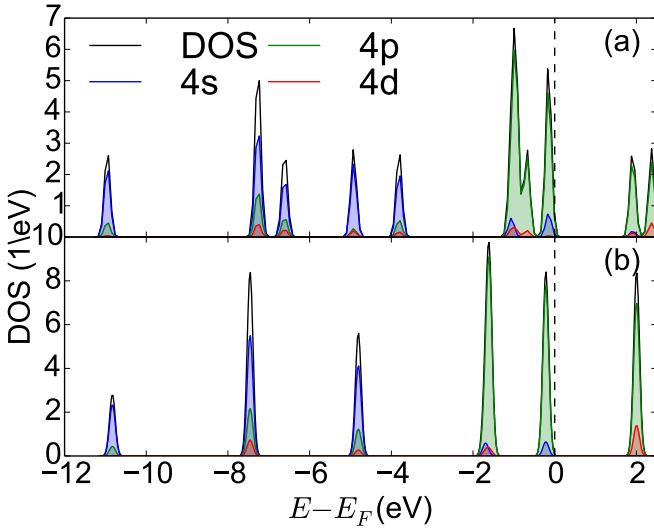


**Fig. 1.** Calculated densities of states (DOS) versus energy (eV) for (a)  $\text{Ge}_6$  and (b)  $[\text{Ge}_6]^{2-}$  where the total DOS is black, the 4s orbital is blue, 4p is green, and 4d is red.

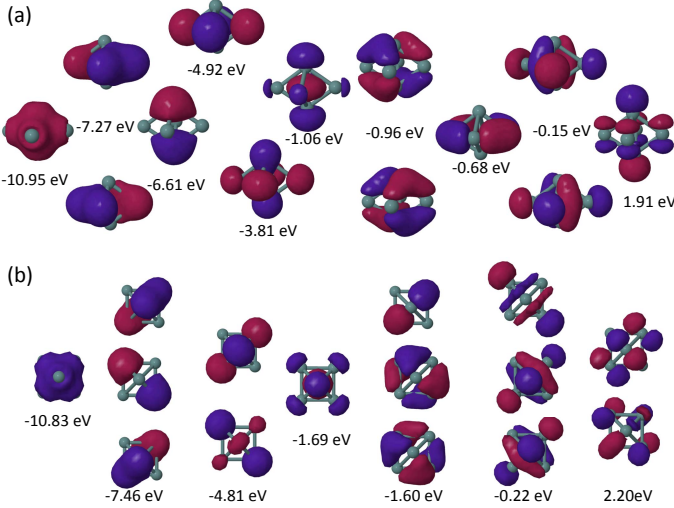


**Fig. 2.** Molecular orbitals of (a)  $\text{Ge}_6$  and (b)  $[\text{Ge}_6]^{2-}$ .

deformations in the geometries, and the known underestimates of  $E_{\text{gap}}$  within GGA calculations, we consider our values reasonable comparisons to previous calculations.

### 3.2 $\text{Ge}_{12}$ Clusters

Zhao *et al.* [?] found the lowest energy isomer of the  $\text{Ge}_{12}$  cluster to be a tetracapped cube with  $C_{2v}$  symmetry, Fig. 3(a). King *et al.* [?] have also studied this cluster and note that it deviates from Wade’s Rules, it is *not* an icosahedron, which would require vertex degrees higher than 4. We also find the same structure found by these authors, with qualitative agreement in the MOs, and the same symmetries and approximate energies levels.

Here we examine the interesting possibility that isomers of  $\text{Ge}_{12}$  may form by joining two  $\text{Ge}_6$  cages together

**Table 1.** Calculated  $E_B$  and  $E_{\text{gap}}$  (eV) of CG-relaxed clusters  $\text{Ge}_6$ ,  $\text{Ge}_9$ , and  $\text{Ge}_{12}$  ( $Z_0$ ) from this work and those of Ref. [?] (in parentheses).

	$\text{Ge}_6$		$\text{Ge}_9$		$\text{Ge}_{12}$ ( $Z_0$ )	
$E_B$	4.425	(3.092)	4.589	(3.215)	4.650	(3.270)
$E_{\text{gap}}$	2.05	(1.992)	1.24	(1.676)	1.59	(2.003)

with one or two intercluster bonds. While these will not result in groundstate  $\text{Ge}_{12}$  clusters, they are analogous to the  $\text{Ge}_9$  chains found experimentally. We initialize each  $\text{Ge}_6$  cluster as an octahedron, again with an initial Ge-Ge separation of 3.0 Å, and change their relative orientation.

Three initial configurations of  $\text{Ge}_6$ - $\text{Ge}_6$  clusters were considered and were named  $\text{I}_n$ ,  $\text{II}_n$ , etc. for their relative energy (after CG relaxation) in the order of highest to lowest binding energy (the notation is general, allowing for clusters that include  $n$  Au atoms). Here we describe the input geometries of the clusters, but their structures can be easily understood from Fig. 3(b-d) since the CG relaxed output geometries differ only slightly from their inputs. Using two local Cartesian coordinate systems  $(x, y, z)$  and  $(x', y', z')$  for each cluster, in configuration  $\text{I}_0$  [Fig. 3 (b)], the axes  $(x, y, z)$  and  $(x', y', z')$  differ by a linear translation so that all axes point respectively in the same directions and the atoms in the two equatorial planes  $xy$  and  $x'y'$  form two intercluster Ge-Ge links pointing locally along directions  $\hat{x} + \hat{y}$  and  $-\hat{x}' - \hat{y}'$ . In configuration  $\text{II}_0$  [Fig. 3 (c)], the two sets of axes again point in the same directions and a single intercluster link forms in the local directions  $\hat{x}$  and  $-\hat{x}'$ . In configuration  $\text{III}_0$  [Fig. 3 (d)], the two octahedra are aligned so that two triangular faces of opposing octahedra are in parallel planes and three intercluster links form a prism.

In Fig. 3 we show the CG-relaxed (first column) and MD “temperature shaken” (second column) geometries of each isomer. MD simulations are started with the CG-relaxed structures shown in Fig. 3 and are run at 600K for 1000 timesteps of 2 fs each [?]. The numbers shown in the figure show the location of each atom through the MD run. The primary differences between CG-relaxed and post-MD structures are small deformations that lead to an overall symmetry loss, as summarized in Table 2 and Table 3. Since Ge-Ge bonds elongate considerably in the cage environment supported with delocalized bonding, we do not attempt to distinguish bonds based on their distances [?].

After CG relaxation, the values of  $E_B$  of all isomers are close to that of the ground state, which we labelled as  $Z_0$  since it is outside our schema of coupled  $\text{Ge}_6$  clusters. We note first that the CG-relaxed  $Z_0$  tetracapped cube has a relatively compact structure including a short Ge-Ge bond of 1.90 Å, and no octahedral structure (and thus we cannot measure  $\bar{d}_G \pm \sigma_{d_G}$  or  $d_i$  in Table 2). It retains much of its symmetry after a MD run. The  $\text{I}_0$ ,  $\text{II}_0$ , and  $\text{III}_0$  clusters built from Wade octahedral  $\text{Ge}_6$  cages

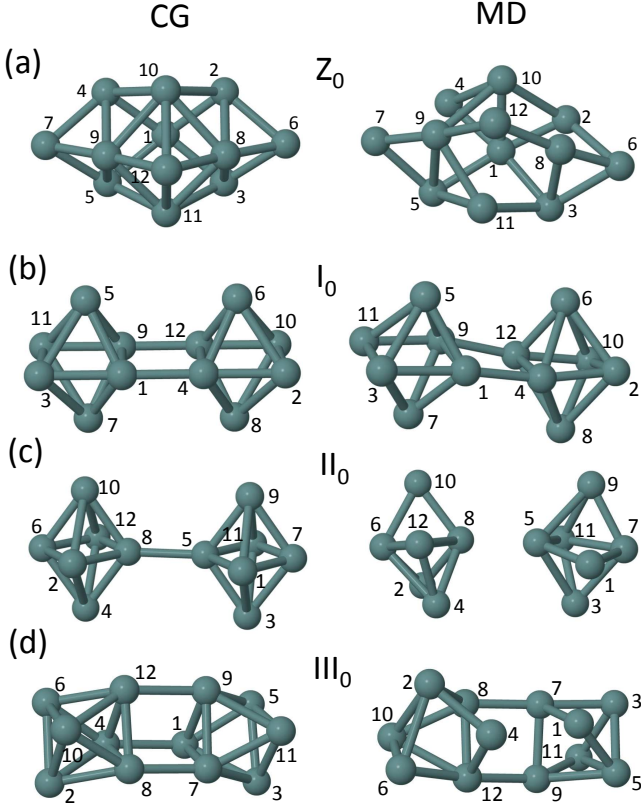


**Fig. 3.**  $\text{Ge}_{12}$  clusters (a)  $Z_0$ ; (b)  $I_0$ ; (c)  $II_0$ ; and (d)  $III_0$ . The left column shows relaxed geometries from CG minimization and the right shows the clusters after a MD run. The structures are all rotated slightly to show the geometry of the interconnections[?].

remain similar to their input geometries and including similar intercluster bonds, or interconnections.  $I_0$  maintains two intercluster bonds  $d_i$  of 2.56 Å.  $II_0$  has the most overall deformation with  $\sigma = 0.182$  Å and maintains one interconnection of length 2.68 Å. Finally  $III_0$  deforms so that it has one strong intercluster bond of  $d_i = 2.64$  Å and two elongated interconnections of  $d_i = 2.80$  Å which are much longer than a typical bulk Ge-Ge bond, but not unusual within a nanocluster or cage geometry.  $II_0$  and  $III_0$  are nearly degenerate energetically, despite their different geometries.

After MD runs,  $I_0$  retains two intercluster bonds and measurably octahedral  $\text{Ge}_6$  cages as shown in Fig. 3(b).  $II_0$  breaks its intercluster bond but its  $\text{Ge}_6$  clusters remain cage-shaped. With structure  $III_0$ , an intercluster bond breaks, and the relative tilting of the two cages has changed. In all cases, the deviation from octahedrality  $\sigma_{d_G}$  is larger in the post-MD structures, the overall symmetry of the cluster is reduced, and the average skeletal Ge-Ge bond length has increased, as quantified in Table 3, which also shows the post-MD bondlengths of  $\text{Ge}_6$  and  $\text{Ge}_6^{2-}$  for comparison.

**Table 2.** Average skeletal distance  $\bar{d}_G$ , deviation from octahedrality  $\sigma_{d_G}$ , range of bond lengths  $d_G$ , intercluster distances  $d_i$  (all distances in Å), and binding energy per atom  $E_B$  (eV) calculated for the CG-relaxed clusters  $\text{Ge}_{12}$ .

$\text{Ge}_{12}$	$\bar{d}_G$	$\sigma_{d_G}$	$d_G$	$d_i$	$E_B$
$Z_0$	—	—	1.90-2.80	—	4.650
$I_0$	2.667	0.104	2.55-2.80	2.56	4.527
$II_0$	2.683	0.182	2.55-2.93	2.68	4.475
$III_0$	2.667	0.064	2.57-2.77	2.64-2.80	4.474

**Table 3.** Calculated average skeletal distances and deviations from octahedrality (Å) of the post-MD clusters  $\text{Ge}_6$ ,  $\text{Ge}_6^{2-}$ , and  $\text{Ge}_{12}$ .

	$(\bar{d}_G)_1$	$(\sigma_{d_G})_1$	$d_G$		
$\text{Ge}_6$	2.72	0.27	2.48-3.36		
$\text{Ge}_6^{2-}$	2.69	0.03	2.63-2.72		
$\text{Ge}_{12}$	$(\bar{d}_G)_1$	$(\sigma_{d_G})_1$	$(\bar{d}_G)_2$	$(\sigma_{d_G})_2$	$d_G$
$Z_0$	—	—	—	—	2.34-3.14
$I_0$	2.721	0.139	2.757	0.173	2.49-3.00
$II_0$	2.710	0.265	2.773	0.360	2.43-3.48
$III_0$	2.767	0.292	2.732	0.278	2.51-3.35

Now we use the DOS (Fig. 4) to examine the stability of CG-relaxed  $\text{Ge}_{12}$  structures. In Fig. 4(a) we present the DOS of  $Z_0$  where the  $4s$  orbitals at  $-6.0 < E - E_F < -4.0$  eV remain well separated with a similar magnitude as neutral  $\text{Ge}_6$ . The  $4p$  states range over  $-4.0 < E - E_F < 0.0$  eV, again of similar magnitude to  $\text{Ge}_6$ , but with a much broader range, indicating the many possible orientations of  $p$  orbitals in a tetracapped cube compared with an octahedron. The placement of the Fermi level at the center of the energy gap indicates this is a stable, insulating cluster.

In Fig. 4(b), for  $I_0$ , we see a similar set of  $4s$  and  $4p$  states below  $E_F$ , with additional states at  $E_F$  itself. These are likely due to the overlap of the two intercluster Ge-Ge bonds. The placement of  $E_F$  indicates these states are metallic. Conversely in Fig. 4(c),  $II_0$  is similar to that of  $\text{Ge}_6$  in Fig. 1(a). While the two highest  $4s$  orbitals remain of similar magnitude to those of the other  $\text{Ge}_{12}$  clusters, like  $\text{Ge}_6$  they are located at  $-4.5 < E - E_F < -3.0$  eV. There is greater symmetry indicated in this cluster, with the  $4p$  orbitals in the range  $-2.5 < E - E_F < 0.0$  eV, and higher/fewer peaks than the other  $\text{Ge}_{12}$  clusters, again much like an individual  $\text{Ge}_6$  cluster. The  $II_0$  cluster is insulating since  $E_F$  is at the base of  $E_{\text{gap}}$  like neutral  $\text{Ge}_6$ .

As was shown with the MD simulation,  $II_0$  is readily broken into two separated  $\text{Ge}_6$  clusters, so it is unsurprising that the overall DOS is qualitatively similar to neutral  $\text{Ge}_6$ . The additional peaks result from more available electronic states in  $\text{Ge}_{12}$  than  $\text{Ge}_6$ , but we observe no states that may be clearly tied to the single intercluster bond.



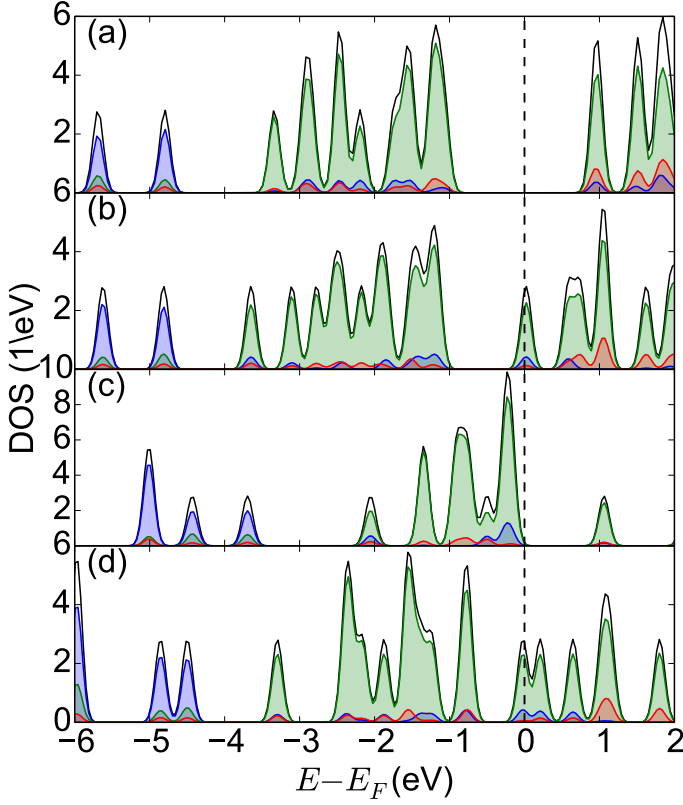


**Fig. 4.** DOS of CG-relaxed  $\text{Ge}_{12}$  isomers: (a)  $Z_0$ , (b)  $I_0$ , (c)  $II_0$ , (d)  $III_0$  (see Fig. 1 for color key).

In Fig. 4(d) we show that  $III_0$  is metallic with many states in  $E_{\text{gap}}$ . The DOS is similar to that of  $I_0$ , yet the  $4s$  states at  $-5.0 < E - E_F < -4.2$  eV are closer together, there are fewer peaks in the  $4p$  orbitals,  $-4.5 < E - E_F < -0.9$  eV, and there is a double peak at  $E_F$ .

We have found COHP electronic partitioning, shown in Figure 5, to be a useful additional tool to determine bond stability (being computationally much less expensive than MD simulations). The groundstate  $Z_0$ , Fig. 5(a), introduces the typical criterion of a stable cluster: the states switch from negative bonding to positive antibonding MOs at the Fermi level. In structure  $I_0$ , Fig. 5(b), the anti-bonding states first appears at  $E_F$  at the top of the band gap. Given the overall stability of this cluster (the two cluster-linking bonds remain stable during MD), this suggests the additional states introduced in the DOS by the intercluster bonds are antibonding, and serve to keep the cluster as two separate, linked structures. Structure  $II_0$ , Fig. 5(c), has antibonding states below  $E_F$  at the base of the energy gap, which can be correlated with the dissociation into two  $\text{Ge}_6$  clusters in the post-MD structure. Cluster  $III_0$ , Fig. 5(d), appears metallic with the first antibonding state at  $E_F$  (much like  $I_0$ ) and a small energy gap. This is consistent with the post-MD rearrangements: the CG-relaxed structure of  $III_0$  has three intercluster bonds and forms two during the MD run. We conclude that two intercluster Ge-Ge bonds provide a relatively stable connecting structure between  $\text{Ge}_6$  octahedral cages.

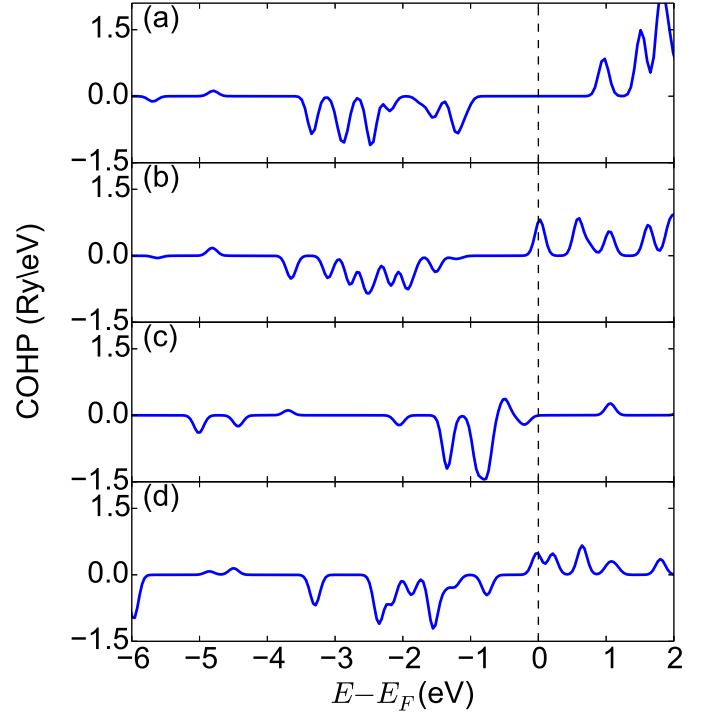


**Fig. 5.** COHP analysis of Ge-Ge interactions  $\text{Ge}_{12}$  after CG relaxation. Structures (a)  $Z_0$ , (b)  $I_0$ , (c)  $II_0$ , and (d)  $III_0$ .

### 3.3 $\text{Au}_3\text{Ge}_{18}$ Clusters

Next we study CG-relaxed structures for  $[\text{Au}_3\text{Ge}_{18}]^{5-}$  and its neutrally charged counterpart in vacuum to compare with the experimentally observed structure. As shown in Fig. 6, this structure consists of two deltahedron-shaped  $\text{Ge}_9$  cages linked by three Au atoms. The three Au atoms bond to three Ge atoms in each cage, forming a prism-like interconnection. Since this figure highlights the interconnection, we mention the asymmetry of the clusters: the apex of one  $\text{Ge}_9$  cage points along an apex of the interconnecting Au-triangle while the opposing cage's apex points in the opposite direction (see Ref. [?]). In comparing the neutral and charged CG-relaxed structures, we observe a very similar intercluster bridge, but the neutrally charged cluster has relatively elongated Ge-Ge bonds [Fig. 6(a)], so that a complete  $\text{Ge}_9$  deltahedron does not form. In Table 4, we summarize our results, comparing them with Spiekermann *et al.* [?], who reported bond lengths from experimental measurements and DFT calculations using a hybrid exchange and correlation (XC) functional. Experimental values for the Au-Au bond lengths, 2.900 to 3.095 Å, are shorter than calculated values. As in experiment, we observe that Ge-Ge bonds adjacent to Ge-Au bonds are considerably shorter than other Ge-Ge bonds. We also compare the three angles  $\theta = \theta_{\text{Ge-Au-Ge}}$  of the intercluster linking prism in the Table 4, finding them to be in reasonable agreement with experiment. We conclude that without the presence of stabilizing ligands SIESTA has successfully reproduced the structures found experimentally.

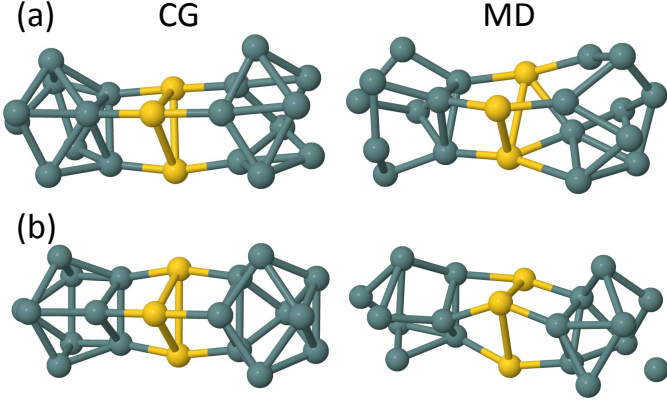


**Fig. 6.**  $\text{Au}_3\text{Ge}_{18}^{q-}$  clusters with charge (a)  $q = 0$  and (b)  $q = 5$ . Au atoms are gold and Ge atoms are gray.

In Fig. 6 we also compare the post-MD structures of  $\text{Au}_3\text{Ge}_{18}$  and  $\text{Au}_3\text{Ge}_{18}^{5-}$  to the CG structures. The neutral cluster forms two additional Au-Ge bonds, and the right hand  $\text{Ge}_9$  cage opens forming a larger cage including the three Au atoms. The  $\text{Au}_3\text{Ge}_{18}^{5-}$  maintains the motif of two  $\text{Ge}_9$  cages separated to an Au triangle since it does not form new Au-Ge bonds. In both clusters the Ge-Ge cage bonds elongate and one Au-Au bond becomes widely separated.

We calculated the binding energy  $E_B$  for the neutral cluster as 4.427 eV, which compares well other calculations in this work. Our calculated  $E_{\text{gap}}$  is considerably smaller than reported by Ref. [?]. Given the superiority of hybrid XC functionals for estimating optical gaps, this is unsurprising. However since our calculations show a stable cluster with a well-separated energy gap with the Fermi level at its base, which indicates overall cluster stability.

In Fig. 7 we present (a) the total DOS and species pDOS, (b) the Ge pDOS of orbitals 4s, 4p, and 4d, and (c) the Au pDOS of orbitals 5d, 6s, and 6p of the neutral cluster. In Fig. 7(a) we see the strongest Au-Ge mixing appears just below  $E_F$  where the Au 5d states mix with the Ge 4p states. Below  $E - E_F < -5.0$  eV the states are dominated by Ge 4s and between  $-5.0 < E - E_F < -2.0$  eV they are dominated by Au 5d states. Here  $E_F$  falls just below a larger gap, indicating a weakly conducting or insulating cluster. In Fig. 7(b) we observe similar Ge orbitals to those in the pure  $\text{Ge}_{12}$  clusters with well separated 4s and 4p states. One sees these 4p orbitals have considerable hybridization and peak at  $E - E_F \approx 1.5$  eV, much like the neutral  $\text{Ge}_6$  cluster. In Fig. 7(c) one sees the 5d orbitals of Au in the region from  $-4.5 < E - E_F < 0.5$  eV, which only strongly mix with the 6s orbital in the range  $-1.5 < E - E_F < 0.5$  eV. The Fermi level is just below  $E_{\text{gap}}$ , indicating a weakly metallic nature in this cluster, and the highest occupied MO is of mainly 4p character, as shown in Fig. S1.

The electronic structure of  $\text{Au}_3\text{Ge}_{18}^{5-}$  is quite similar to the neutral cluster, however  $E_F$  sits at the top of  $E_{\text{gap}}$ , which indicates it is unstable without external ligands. Indeed, as shown in Fig. 6, we observed considerable rearrangement of both neutral and charged clusters under

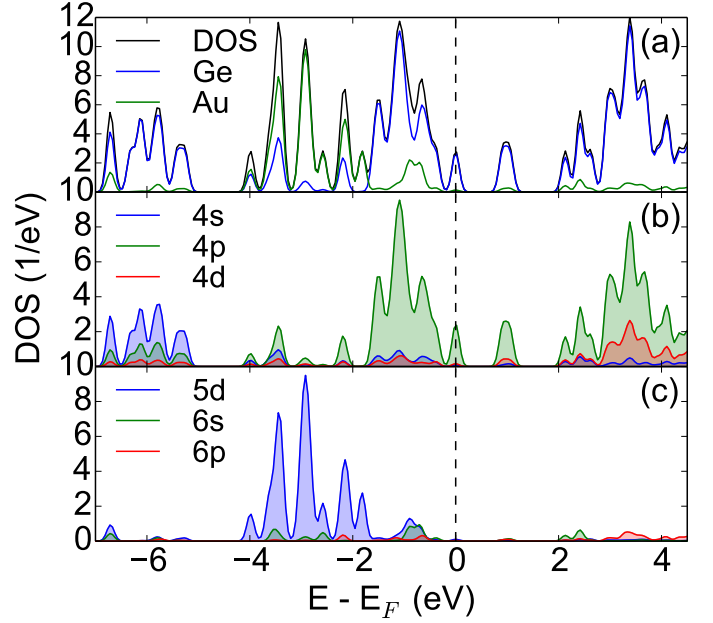


**Fig. 7.** The electronic structure of  $\text{Au}_3\text{Ge}_{18}$  (neutrally charged) (a) DOS (black), Ge pDOS (blue) and Au pDOS (green), (b) Ge 4s (blue), 4p (green), and 4d (red), and (c) Au 5d (blue), 6s (green), and 6p (red).

**Table 4.** Ranges of calculated bond lengths ( $\text{\AA}$ ) found for Ge, Au-Ge, and Au-Au bonds for  $[\text{Au}_3\text{Ge}_{18}]^{q-}$ . Also shown, values for the angles  $\theta$  connecting Au to the two cages.

$q$	$d_G$	$d_{AG}$	$d_A$	$\theta$	Ref.
0	2.5-2.85	2.46-2.48	3.11-3.19	$165^\circ$ - $174^\circ$	
5-	2.56-2.86	2.53	3.03-3.34	$165^\circ$ - $172^\circ$	
5-	2.55-2.88	2.45-2.46	2.900-3.095	$168^\circ$ - $174^\circ$	[?]

MD simulation, which restores the electronic structure to a stable configuration. Like its neutral counterpart, the pDOS of  $\text{Au}_3\text{Ge}_{18}^{5-}$  shows orbitals dominated by 4s character below  $E - E_F = -2.0$  eV and by 4p in the range  $-2.0 \text{ eV} < E - E_F < 0.0 \text{ eV}$ . This is the characteristic orbital behavior in both pure Ge clusters and Au-Ge clusters which we observe through this study.

In the COHP analysis of the neutral  $\text{Au}_3\text{Ge}_{18}$ , Fig. 8, we note three features: in (a) the Au-Au interaction has strong antibonding states at  $E_F$ ; in (b) Au-Ge has a weak antibonding state at  $E_F$  (this disappears in the post-MD structure); and in (c) Ge-Ge is bonding up to  $E_F$ , and antibonding above. At this level of theory, it appears Ge-Ge interactions are the strongest indicator of stability.

### 3.4 $\text{Au}_n\text{Ge}_{12}$ Clusters

Now we examine linked  $\text{Ge}_6\text{Au}_n\text{Ge}_6$  configurations to compare with  $\text{Au}_3\text{Ge}_{18}$ . There are innumerable combinations of two octahedral  $\text{Ge}_6$  cages connected to one or more Au

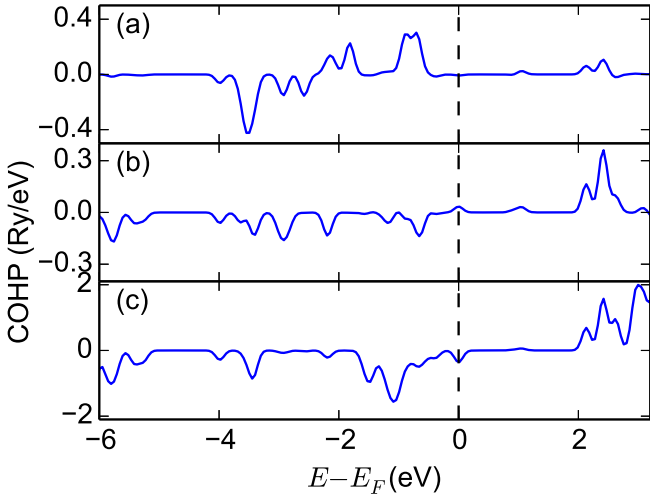


**Fig. 8.** COHP for  $\text{Au}_3\text{Ge}_{18}$  where for interactions (a) Au-Au, (b) Au-Ge, and (c) Ge-Ge.

atoms, so we design input geometries to test the linearity of Ge-Au-Ge links and accommodate the symmetries of the  $\text{Ge}_6$  cages. A basic question is when will there be sufficient electrons such that the cages maintain the octahedral symmetry of the Wade-like  $\text{Ge}_6^{2-}$  clusters and also bond together through the gold interconnections. We ran CG relaxations of many such input geometries, but illustrate just a few of the most interesting cases which have similar initial  $\text{Ge}_6$  orientations as those described in Section 3.2, now with intercluster Au atoms.

With just one Au atom, we examined orientations very similar to the CG structures  $\text{I}_0$  and  $\text{II}_0$  with an Au atom added. For both of these orientations, the axes of the octahedra are aligned with an Au atom at their midpoint. The input structure for  $\text{I}_0$  produced  $\text{I}_1$ , where a total of four Au-Ge links could form in the equatorial planes of the two octahedra. Likewise  $\text{II}_0$  and  $\text{II}_1$  shared input structures where the added Au atom in  $\text{II}_1$  created two Au-Ge links in a line connecting the apexes of the two octahedra. With two Au atoms, many possible interlinked combinations exist, but stable isomers resulted from placing both Au atoms in the common equatorial plane of the two octahedra, creating four Au-Ge links. With three Au atoms, we focused on canted octahedra, similar to structure  $\text{III}_0$  [Fig. 3(c)], to create a nine-atom prism much like that in  $\text{Au}_3\text{Ge}_{18}$ .

Such initialization procedures requires an exploration of geometry phase space to ensure our CG relaxations do not find highly metastable states. In order to sample many possible configurations we use a “geometry sweep” much like the approach used to find the groundstate of crystal structures in DFT methods. In general, a sweep was generated by using as a variable the *initial* separation  $d_{\text{init}}$  of Au from Ge atoms to which it was interconnected. For a given initial cluster orientation, independent CG relaxations of the cluster were run for a series of Au-Ge separations, yielding many isomers to compare, each with a

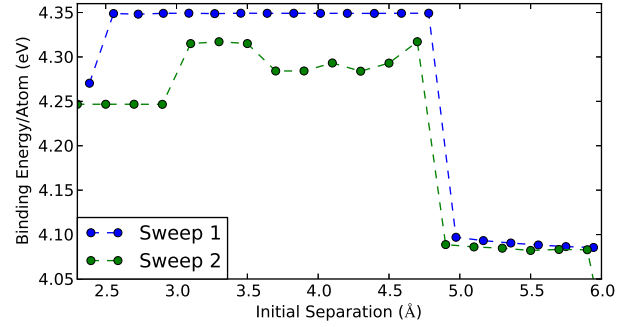


**Fig. 9.** Geometry sweep for clusters  $\text{AuGe}_{12}$ : where the CG-relaxed geometry and corresponding  $E_B$  (eV) are shown as a function of initial Au-Ge separation. The input structures of Sweep 1 and 2 are described in the text.

relaxed geometry and binding energy. A single geometry sweep explored one input orientation with 15-20 different Au-Ge separations while setting initial Ge-Ge distances at 3.0 Å. The CG relaxations returned dense clusters with high binding energies for short Au-Ge distances, dissociated clusters with low binding energies at long Au-Ge distances, and intermediate clusters which retained two  $\text{Ge}_6$  cages connected by Au atoms. Generally within a broad range of  $d_{\text{init}}$ , these intermediate clusters are nearly identical after CG relaxation. From these intermediate isomers we present those with relatively high binding energies.

Figure 9 shows two geometry sweeps for  $\text{AuGe}_{12}$ , where each point represents a separate isomer. Each sweep produces compact clusters at  $d_{\text{init}} < 2.5$  Å, intermediate clusters at  $2.5 < d_{\text{init}} < 5.0$  Å, and dissociated clusters at higher separations. Sweep 1, with four Au-Ge interconnects, produces  $\text{I}_1$  in the range  $2.5 < d_{\text{init}} < 5.0$  Å, and yields low  $E_B$  structure  $\text{V}_1$  at  $d_{\text{init}} = 2.5$  Å. Sweep 2, with two Au-Ge interconnects, produces many isomers:  $\text{II}_1$ - $\text{III}_1$  observed where  $3.0 < d_{\text{init}} < 3.6$  Å,  $\text{IV}_1$  in the range  $3.8 < d_{\text{init}} < 4.8$  Å, and  $\text{VI}_1$  and  $\text{VII}_1$  at  $2.2 < d_{\text{init}} < 3.0$  Å. We show the geometries of  $\text{I}_1$  and  $\text{II}_1$  in Fig. 10 and  $\text{III}_1$ - $\text{VII}_1$  in Fig. S2. The geometry differences within a sweep are small and the overall range of  $E_B/\text{atom}$  between isomers is less than 0.1 eV, indicating near degeneracy of the clusters. Interesting differences include those of  $\text{II}_1$  and  $\text{III}_1$ , where  $\text{III}_1$  is twisted about its long axis compared with  $\text{II}_1$ .  $\text{V}_1$  is considerably more octahedral than  $\text{I}_1$ .

In each group  $\text{Au}_n\text{Ge}_{12}$ ,  $n = 1 - 3$ , we identified a few highest binding energy structures for careful study and present geometry and energy data of their CG relaxations in Table 5 and those for post-MD in Table 6. We examine clusters which maintain a recognizable pair of  $\text{Ge}_6$  cages throughout a CG relaxation. Differences in energies between the highest and lowest in each group was small, typically less than 0.1 eV. There are no significant trends in the deviation from octahedrality  $\sigma_{d_G}$  with binding energy. Ge-Au-Ge angles  $\theta$  vary from straight to bent (e.g., there is one structure,  $\text{II}_3$ , in the  $\text{Au}_3\text{Ge}_{12}$  series that has a near tetrahedral angle). Due to the large number of CG-relaxed  $\text{Au}_n\text{Ge}_{12}$  structures summarized in this table, we



**Table 5.** Calculated average skeletal distances ( $\text{\AA}$ ) and deviations from octahedrality ( $\text{\AA}$ ) of the CG-relaxed clusters  $\text{Au}_n\text{Ge}_{12}$  shown in Figs. 10 and S2. Also shown, ranges for bond lengths  $d_G$ ,  $d_{AG}$ ,  $d_A$ , and values for the angles  $\theta$  connecting Au to the two cages and energy  $E_B$  (eV).

$\text{AuGe}_{12}$	$\bar{d}_G$	$\sigma_{d_G}$	$d_{AG}$		$d_G$	$\theta$	$E_B$
I <sub>1</sub>	2.731	0.242	2.66		2.58-3.29	104°	4.349
II <sub>1</sub>	2.663	0.127	2.46		2.53-2.86	180°	4.317
III <sub>1</sub>	2.664	0.127	2.465		2.51-2.88	180°	4.315
IV <sub>1</sub>	2.689	0.189	2.49		2.55-2.94	180°	4.284
V <sub>1</sub>	2.703	0.086	2.53		2.54-2.77	114°	4.270
VI <sub>1</sub>	2.673	0.124	2.49		2.57-2.83	180°	4.266
VII <sub>1</sub>	2.652	0.028	2.46		2.63-2.69	180°	4.247
$\text{Au}_2\text{Ge}_{12}$	$\bar{d}_G$	$\sigma_{d_G}$	$d_{AG}$	$d_A$	$d_G$	$\theta$	$E_B$
I <sub>2</sub>	2.735	0.343	2.46-2.51	2.89	2.50-3.76	171.4°-176°	4.292
II <sub>2</sub>	2.837	0.443	2.42-2.52	2.90	2.48-3.83	117-176°	4.291
III <sub>2</sub>	2.709	0.232	2.52-2.64	2.81	2.52-3.14	172.5°	4.256
IV <sub>2</sub>	2.654	0.063	2.46	4.09	2.57-2.72	148°	4.241
$\text{Au}_3\text{Ge}_{12}$	$\bar{d}_G$	$\sigma_{d_G}$	$d_{AG}$	$d_A$	$d_G$	$\theta$	$E_B$
I <sub>3</sub>	2.653	0.063	2.46-2.50	4.15	2.56-2.71	130 – 138°	4.191
II <sub>3</sub>	2.661	0.048	2.49-2.81	3.45-3.59	2.58-2.73	109 – 175°	4.187
III <sub>3</sub>	2.685	0.056	2.48-2.52	3.06	2.62-2.76	136 – 151°	4.181
IV <sub>3</sub>	2.683	0.142	2.50-2.54	2.97	2.51-2.93	112 – 139°	4.145
V <sub>3</sub>	2.760	0.356	2.51-2.69	2.78-2.94	2.52-3.74	174°	4.135

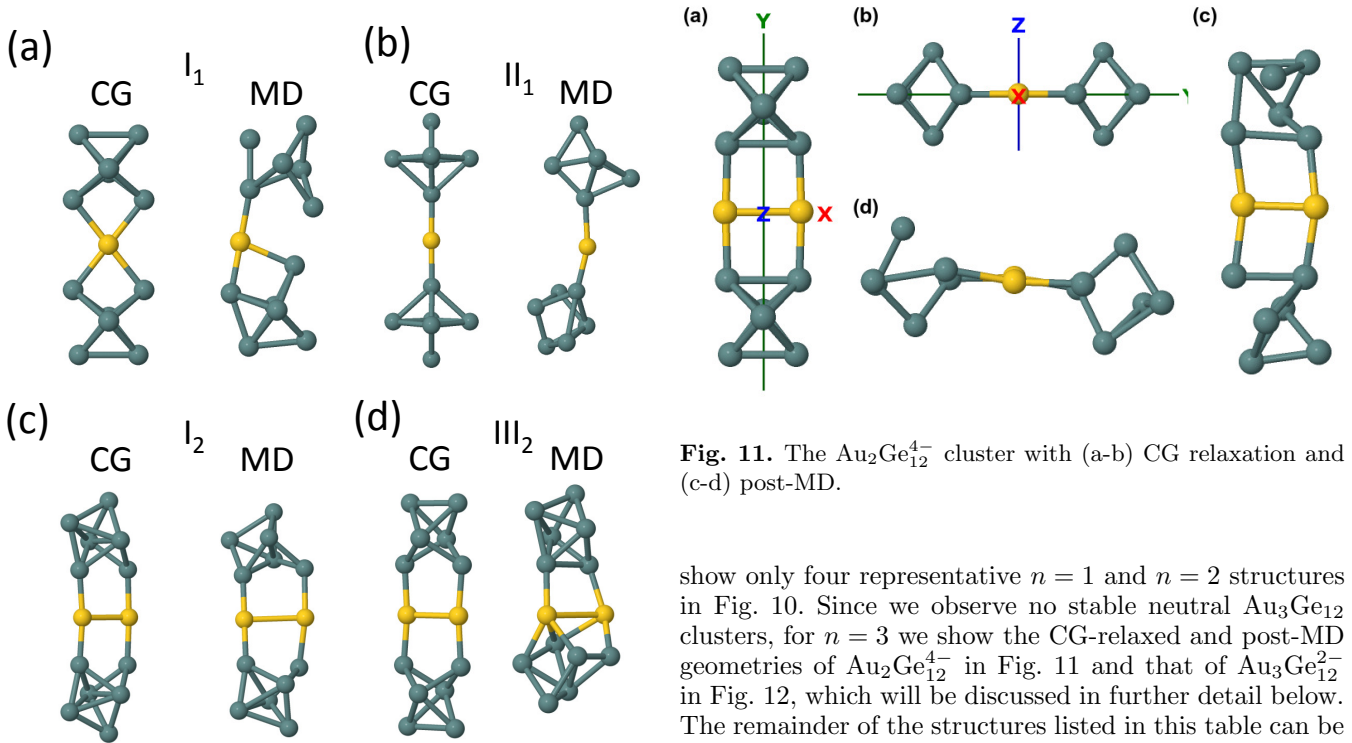


**Fig. 10.** Examples of  $\text{Au}_n\text{Ge}_{12}$  clusters after CG relaxation (left) and post-MD (right). (a)  $n = 1$ , structure I<sub>1</sub>; (b)  $n = 1$ , structure II<sub>1</sub>; (c)  $n = 2$ , structure I<sub>2</sub>; (d)  $n = 2$ , structure III<sub>2</sub>. Au atoms are gold and Ge are gray.

**Fig. 11.** The  $\text{Au}_2\text{Ge}_{12}^{4-}$  cluster with (a-b) CG relaxation and (c-d) post-MD.

show only four representative  $n = 1$  and  $n = 2$  structures in Fig. 10. Since we observe no stable neutral  $\text{Au}_3\text{Ge}_{12}$  clusters, for  $n = 3$  we show the CG-relaxed and post-MD geometries of  $\text{Au}_2\text{Ge}_{12}^{4-}$  in Fig. 11 and that of  $\text{Au}_3\text{Ge}_{12}^{2-}$  in Fig. 12, which will be discussed in further detail below. The remainder of the structures listed in this table can be found in Fig. S2.

Figure 10 compares  $n = 1$  isomers (a) I<sub>1</sub> and (b) II<sub>1</sub> that have respectively four and two Ge-Au-Ge intercluster links after CG relaxation. The octahedra of I<sub>1</sub> are more deformed than II<sub>1</sub>, with  $\sigma_{d_G}$  larger by 0.12  $\text{\AA}$ , the Au-Ge bonds are longer in I<sub>1</sub> by 0.2  $\text{\AA}$ , and  $E_B$  is greater by approximately 0.03 eV. Post-MD, we see I<sub>1</sub> (a) breaks an Au-Ge intercluster bond, while II<sub>1</sub> (b) maintains both:

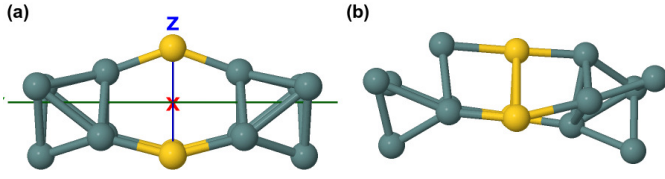


**Fig. 12.** The  $\text{Au}_3\text{Ge}_{12}^{2-}$  cluster with (a) CG relaxation and (b) post-MD. The three Au atoms form a triangle in the x-z plane, and the lower, back Au atom is hidden from view.

merely twisting about its Ge-Au-Ge intercluster link so  $\theta_{\text{Ge-Au-Ge}}$  remains close to linear. When comparing the two predominant isomers of  $\text{AuGe}_{12}$ , the four Au-Ge intercluster bonds of  $\text{I}_1$  are less stable than the two of  $\text{II}_1$ .

For  $n = 2$ , Fig. 10 compares the isomers (c)  $\text{I}_2$  and (d)  $\text{III}_2$ . After CG relaxation,  $\text{I}_2$  is less symmetric than  $\text{III}_2$  ( $C_{2v}$  vs.  $D_{2h}$ ) which coincides with reduced octahedrality in  $\text{I}_2$  ( $\sigma_{d_G} = 0.343 \text{ \AA}$ ).  $\text{II}_2$  (Fig. S2) is similar to  $\text{I}_2$ , with more exaggerated asymmetry ( $\sigma_{d_G} = 0.443 \text{ \AA}$ ), while  $\text{IV}_2$  (Fig. S2) is similar to  $\text{III}_2$  with a strongly bent Ge-Au-Ge link ( $172.5^\circ$  vs  $148^\circ$ ) and a widely separated Au-Au distance ( $4.09 \text{ \AA}$ ). The overall symmetry change between the isomers of  $\text{Au}_2\text{Ge}_{12}$  appears to have direct consequences for the overall cluster stability. The stability for  $n = 2$  under MD simulation appears to rely more on symmetry than number of intercluster links: the asymmetric  $\text{I}_2$  and  $\text{II}_2$  structures are stable under MD while the relatively symmetric  $\text{III}_2$  and  $\text{IV}_2$  structures are not although each have four linear Au-Ge intercluster links. This is consistent with the asymmetric coupling of the  $\text{Ge}_9$  clusters in  $[\text{Au}_3\text{Ge}_{18}]^{5-}$ . We see that  $\text{Au}_3\text{Ge}_{12}$  does not readily form linear stable Ge-Au-Ge links, whether the relative  $\text{Ge}_6$  orientations are symmetric or asymmetric.

Charge influences cluster shape, as dictated by Wade's rules. We consider here the effect of a charge  $q = 2$  and  $q = 4$  on some isomers of  $\text{Au}_n\text{Ge}_{12}^{q-}$ . To obtain these results, we ran identical geometry sweeps to our neutral charge calculations, with charge  $q = 2$  and  $q = 4$  added to the cluster.

Table 7 lists two stable isomers that were found for  $\text{Au}_2\text{Ge}_{12}^{2-}$ . The primary difference is in the linearity of the Ge-Au-Ge links and the degree of octahedrality, with lower energy isomer having  $\theta = 148.5^\circ$ , like the neutral  $\text{IV}_2$ , and  $\sigma_{d_G} = 0.05 \text{ \AA}$ . Nearly degenerate is the isomer with  $\theta = 178.5^\circ$ , like the neutral  $\text{III}_2$ . When the charge is increased to  $q = 4$ , only the linear-link isomer is observed, which is also stable under MD simulation. Likewise we observed a stable isomer of  $\text{Au}_3\text{Ge}_{12}^{q-}$  with both  $q = 2$  and  $q = 4$ . While the CG-relaxed  $\text{Au}_3\text{Ge}_{12}^{2-}$  still has bent Ge-Au-Ge links ( $\theta = 140^\circ - 149^\circ$ ), the post-MD structure has one nearly linear bond ( $\theta = 178^\circ$ ), and the bridging structure resembles a prism. This structure type was simply not observed in the neutral cluster.

In contrast to the neutrally charged isomers, we observe linear links in both  $\text{Au}_2\text{Ge}_{12}^{q-}$ ,  $q = 2$  and  $q = 4$  with  $D_{2h}$  symmetry (as  $\text{III}_2$ ) that are stable under MD simulation. Moreover we observe stable  $\text{Au}_3\text{Ge}_{12}^{q-}$  clusters.

While a more complete exploration of both value of  $q$  and possible linking structures could be performed, this work confirms that additional charge stabilizes linear Ge-Au-Ge cluster interconnections.

The DOS of the  $\text{Au}_n\text{Ge}_{12}$  clusters generally resembles that of  $\text{Au}_3\text{Ge}_{18}$  where the Ge  $4p$  orbitals dominate just below  $E_F$  with some overlap with the Au  $5d$  states. The Ge  $4p$  and Au  $5d$  states of  $\text{I}_1$  have less overlap than  $\text{II}_1$ . The DOS of  $\text{I}_2$  and  $\text{III}_2$  are qualitatively similar, but the additional symmetry of  $\text{III}_2$  promotes  $E_F$  above the energy gap of  $\text{I}_2$ , indicating an electronic instability. We see the most overlap between Ge and Au orbitals in  $\text{Au}_3\text{Ge}_{12}$  due to the greater magnitude of the Au states, but it is clear from MD that this does not contribute to a stability of the  $\text{Ge}_6\text{Au}_n\text{Ge}_6$  motif when  $n = 3$ . We present the HOMO and LUMO of selected  $\text{Au}_n\text{Ge}_{12}$  clusters in Figs. S3-S7 where delocalized bonding is apparent in the LUMO states of  $n = 1, 3$  and the HOMO states in  $n = 2$   $\text{Au}_n\text{Ge}_{12}$  clusters.

In COHP analysis, we use the structures shown in Fig. 10 to compare the properties of stable CG-relaxed  $\text{Au}_n\text{Ge}_{12}$  clusters:  $\text{I}_1$  and  $\text{II}_1$  in  $\text{AuGe}_{12}$  and  $\text{I}_2$  and  $\text{III}_2$  in  $\text{Au}_2\text{Ge}_{12}$ . We show their COHP interactions in three figures: Ge-Ge in Fig. 13; Au-Ge in Fig. 14; and Au-Au in Fig. 15. Generally we see that the primary indicator of stability is that of the Au-Ge interaction.

In  $\text{AuGe}_{12}$  the overall similarities between  $\text{I}_1$  and  $\text{II}_1$  in the the Ge-Ge interaction are apparent in Fig. 13 (a-b) respectively where a single, large bonding peak appears below  $E_F$  at  $E - E_F \approx -2.0 \text{ eV}$ . However  $\text{I}_1$  shifts from Ge-Ge bonding to antibonding states at  $E_F$  while  $\text{II}_1$  has a small antibonding state in Ge-Ge at  $E_F$ . In the Au-Ge interaction [Fig. 14 (a-b)],  $\text{I}_1$  has antibonding states at  $E_F$ , while  $\text{II}_1$  has no Au-Ge state at  $E_F$ . Instead  $E_F$  is centered between occupied bonding and empty antibonding states. Given our observations during MD simulation that  $\text{I}_1$  is less stable, this indicates the Ge-Ge antibonding state arises from intercluster interaction, like that of  $\text{I}_0$ , but does not break the structure. The antibonding Au-Ge state at  $E_F$  of  $\text{I}_1$  is likely to cause the Au-Ge bond breaking observed in the post-MD cluster, whereas those in  $\text{II}_1$ , with no such antibonding interaction, merely twist, but remain bonded.

The Ge-Ge COHP curves of  $\text{Au}_2\text{Ge}_{12}$   $\text{I}_2$  and  $\text{III}_2$  are qualitatively similar to one another [Figs. 13(c,d)]. Neither cluster has antibonding states below  $E_F$ , and the primary difference is the shift in the location of  $E_F$  from  $\text{I}_2$  to  $\text{III}_2$ . Significantly, while the Au-Ge interactions of  $\text{I}_2$  have no antibonding character below  $E_F$  [Fig. 14(c)], there is an antibonding interaction in  $\text{III}_2$  [Fig. 14(d)], again confirming that antibonding states in Au-Ge below  $E_F$  are correlated with cluster instability. In examining COHP curves of  $\text{Au}_3\text{Ge}_{12}$ , there are as many as three antibonding states below  $E_F$  in Au-Ge interactions, thus it is unsurprising that no neutral stable clusters were observed.

We see no overall stability trends in the Au-Au COHP results. In Fig. 15 we show the Au-Au COHP results of (a)  $\text{I}_2$  and (b)  $\text{III}_2$ . In both cases, there are significant antibonding MO's below  $E_F$ . In terms of antibonding states,

**Table 6.** Results for the calculated average skeletal distances and deviations from octahedrality ( $\text{\AA}$ ) of the  $\text{Au}_n\text{Ge}_{12}$  clusters after MD runs, where a blank in a  $\sigma_{d_G}$  column indicates a complete disordering of the octahedra. Also shown, values for the angles  $\theta$  connecting Au to the two cages and energy,  $E_B$  (eV). Structures are shown in Figs. 10 and S2.

$\text{AuGe}_{12}$		$d_{AG}$	$\theta$	$(\bar{d}_G)_1$	$(\sigma_{d_G})_1$	$(\bar{d}_G)_2$	$(\sigma_{d_G})_2$	$d_G$
I <sub>1</sub>		2.46, 2.76	166°	2.74	0.32	2.79	0.40	2.36-3.51
II <sub>1</sub>		2.45, 2.60	163°	2.74	0.40	2.73	0.23	2.42-3.95
$\text{Au}_2\text{Ge}_{12}$	$d_A$	$d_{AG}$	$\theta$	$(\bar{d}_G)_1$	$(\sigma_{d_G})_1$	$(\bar{d}_G)_2$	$(\sigma_{d_G})_2$	$d_G$
I <sub>2</sub>	3.20	2.49-2.66	163°, 177°	2.779	0.379	2.743	0.309	2.53-3.73
II <sub>2</sub>	3.03	2.47-2.73	173°	2.774	0.318	2.812	0.409	2.43-3.87
III <sub>2</sub>	3.42	2.41-2.84	102°-157°	2.696	0.298	—	—	2.39-3.56
IV <sub>2</sub>	3.27	2.38-2.73	125°-163°	2.726	0.251	—	—	2.49-3.41
$\text{Au}_3\text{Ge}_{12}$	$d_A$	$d_{AG}$	$\theta$	$(\bar{d}_G)_1$	$(\sigma_{d_G})_1$	$(\bar{d}_G)_2$	$(\sigma_{d_G})_2$	$d_G$
I <sub>3</sub>	3.04	2.46-3.04	75° – 169°	—	—	—	—	2.52-3.21
II <sub>3</sub>	3.60-3.71	2.48-3.01	100° – 175°	2.68	0.11	—	—	2.54-2.99
III <sub>3</sub>	3.25-3.68	2.43-2.91	96° – 165°	2.81	0.28	—	—	2.54-3.53
IV <sub>3</sub>	2.75	2.45-2.89	127° – 143°	2.73	0.19	—	—	2.37-3.29
V <sub>3</sub>	2.77	2.48-2.84	150°	2.81	0.37	—	—	2.51-3.83

**Table 7.** Calculated properties of the CG-relaxed clusters found in geometry sweeps for charged clusters  $\text{Au}_n\text{Ge}_{12}^{q-}$ . Also shown, the properties for these clusters post-MD.

CG Properties						
	$\bar{d}_G$	$\sigma_{d_G}$	$d_{AG}$	$d_A$	$d_G$	$\theta$
Au <sub>2</sub> Ge <sub>12</sub> <sup>2-</sup> (1)	2.66	0.05	2.49	3.92	2.56-2.73	148.5°
Au <sub>2</sub> Ge <sub>12</sub> <sup>2-</sup> (2)	2.70	0.15	2.53	2.84	2.53-2.95	178.5°
Au <sub>2</sub> Ge <sub>12</sub> <sup>4-</sup>	2.72	0.09	2.59	2.89	2.51-2.84	176°
Au <sub>3</sub> Ge <sub>12</sub> <sup>2-</sup>	2.67	0.06	2.58-2.75	3.14-4.0	2.51-2.84	140° – 149°
Au <sub>3</sub> Ge <sub>12</sub> <sup>4-</sup>	2.73	0.13	2.76	3.23-3.72	2.59-2.93	155°
MD Properties						
	$\bar{d}_G$	$\sigma_{d_G}$	$d_{AG}$	$d_A$	$d_G$	$\theta$
Au <sub>2</sub> Ge <sub>12</sub> <sup>2-</sup> (1)	2.67	0.11	2.46-2.48	3.80	2.35-4.05	140°,157°
Au <sub>2</sub> Ge <sub>12</sub> <sup>2-</sup> (2)	2.72	0.23	2.38-2.60	3.82	2.40-2.88	149°,157°
Au <sub>2</sub> Ge <sub>12</sub> <sup>4-</sup>	2.79	0.17	2.62-2.70	2.76	2.51-3.26	161° – 164°
Au <sub>3</sub> Ge <sub>12</sub> <sup>2-</sup>	2.75	0.15	2.37-2.73	3.22-3.96	2.43-2.99	146° – 178°
Au <sub>3</sub> Ge <sub>12</sub> <sup>4-</sup>	2.82	0.24	2.58	2.93-4.16	2.58-3.39	135° – 171°

the Au-Au COHP for  $\text{Au}_2\text{Ge}_{12}$ , is consistent with that observed for the charged  $\text{Au}_3\text{Ge}_{18}^{5-}$ . To further examine this antibonding state the electronic structure analysis should account for aurophilic Au-Au interactions as discussed in Refs. [?, ?].

### 3.5 Extended $\infty[\text{Au}_2\text{Ge}_6]$ Structures

To extend our exploration of the ability of  $\text{Ge}_6$  cages to bond with Au atoms, we consider crystalline Au-Ge structures built with this geometry. The precedent studies include Ref. [?], where 1D, 2D, and 3D structures formed of  $\text{Ge}_9$  cages were examined. We show the hypothetical structure  $\infty[\text{Au}_2\text{Ge}_6]$  in the inset of Fig. 16 which rep-

resents the isomer observed with binding energy maximum at  $d_{\text{init}} = 2.6 \text{ \AA}$ . Here, Au atoms are placed in the positions of the radial non-bonding orbitals of isolated  $[\text{Ge}_6]^{2-}$  clusters in the  $xy$  plane. Following the techniques of Sec. 3.4, we vary the initial Au-Ge distance, perform CG minimization, and find the binding energy and relaxed geometry (Fig. 16). The relaxed structure features a subunit of a  $\text{Ge}_6$  octahedron with four radial Au-Ge bonds. Each subunit is spaced closely to form a 2D crystal structure including Au-Au bonds. The binding energy has a peak at  $d_{\text{init}} = 2.6 \text{ \AA}$ , where  $d_{\text{init}}$  is the initial Au-Ge bondlength. The average bond found in the Ge cages is  $\bar{d}_G = 2.72 \pm 0.06 \text{ \AA}$ , showing that the bonds are elongated compared to the isolated clusters, but the cages are close to octahedral. Ge-Ge bonds

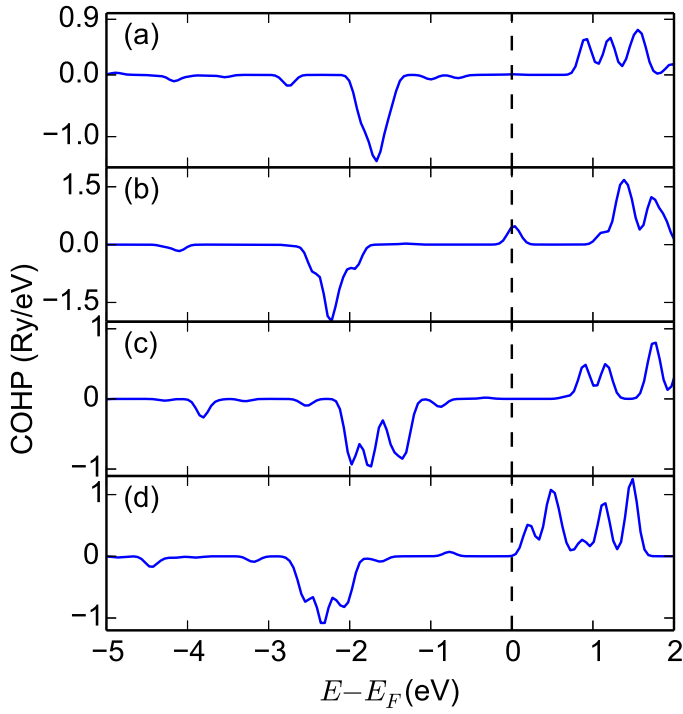


**Fig. 13.** COHP for Ge-Ge bonds for  $\text{Au}_n\text{Ge}_{12}$  where (a)  $I_1$ , (b)  $II_1$ , (c)  $I_2$ , (d)  $III_2$

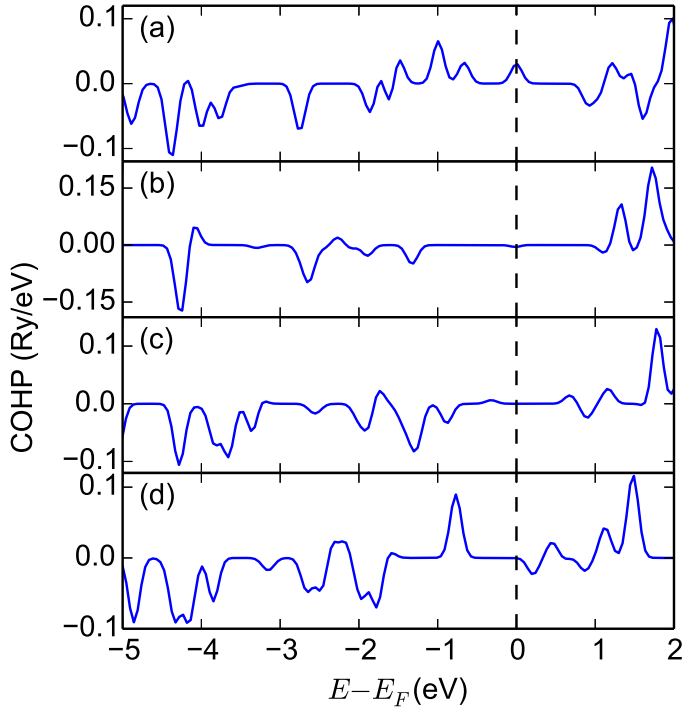


**Fig. 14.** COHP for Au-Ge bonds for  $\text{Au}_n\text{Ge}_{12}$  where (a)  $I_1$ , (b)  $II_1$ , (c)  $I_2$ , (d)  $III_2$ .

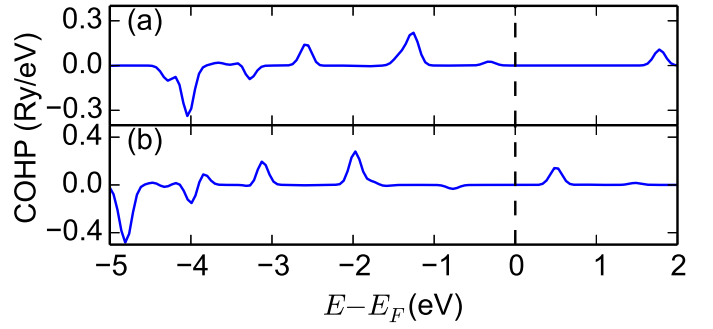


**Fig. 15.** COHP for Au-Au bonds for  $\text{Au}_2\text{Ge}_{12}$ , where (a)  $I_2$ , (b)  $III_2$ .

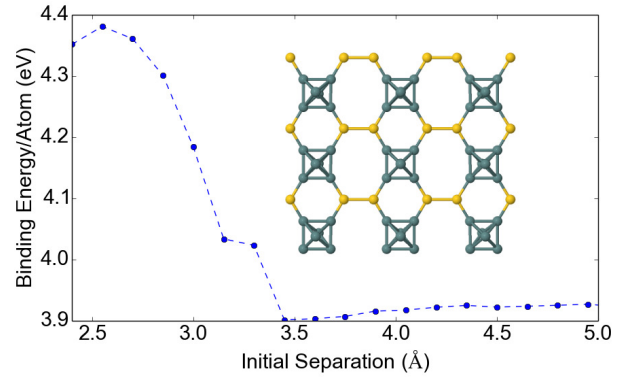


**Fig. 16.** Binding energy  $E_B$  (eV) versus  $d_{\text{init}}$  (Å) of extended structure  $2[\text{Au}_2\text{Ge}_6]$ . The inset shows the geometry of this local  $E_B$  maxima found with CG minimization for  $d_{\text{init}} = 2.6$  Å.

range from  $d_G = 2.62 - 2.77$  Å, which includes those in the two-dimensional plane forming a square with lengths of approximately 2.65 Å and the out-of-plane bonds are 2.77 Å. The Au-Ge bond lengths  $d_A = 2.42$  Å are short compared with the clusters studied in Sec. 3.2 and the Au-Au bond is  $d_A = 2.85$  Å. The Ge-Au-Ge linking angle is  $117^\circ$ . We explored other stoichiometries, such as  $1[\text{Au}_1\text{Ge}_6]$ ,  $1[\text{Au}_2\text{Ge}_6]$ , and  $2[\text{Au}_4\text{Ge}_6]$ , and observed considerably less smooth  $E_B$  vs.  $d_{\text{init}}$  curves, indicating these stoichiometries prefer dissociation or non-octahedral geometries in the input structures we examined. Again we see that a Au-Ge ratio of 1:6 seems to support greater overall stability in Au-Ge systems.

## 4 Discussion and Conclusions

Beyond its well known properties as a covalently bonded  $sp^3$  semiconductor, the versatility in the Ge electronic structure allows it to form cage-like structures with extended bond lengths. Taken in isolation, cages  $\text{Ge}_6$  and  $\text{Ge}_9$  need additional electrons to stabilize their deltahe-dral shapes; two electrons being sufficient for the former, and four for the latter, consistent with Wade's Rules. By using DFT methods, we have examined the stability of combinations of octahedral  $\text{Ge}_6$  cages in various forms. In examining linking structures between two such cages, we

found that two bonds form and stabilize  $\text{Ge}_{12}$ , especially when the two clusters are aligned symmetrically with Ge-Ge bonds connecting the two equatorial planes of the octahedra. Other orientations are less stable, as can be seen using COHP analysis or by running brief MD simulations to examine how the cluster evolves.

By combining Au with Ge, new possibilities emerge. It is tantalizing that through linking to a triangle of Au atoms, deltahedral  $\text{Ge}_9$  cages stabilize in the charged  $[\text{Au}_3\text{Ge}_{18}]^{5-}$ . In analogy, this paper addressed whether  $\text{Ge}_6$  cages could be linked into  $\text{Au}_n\text{Ge}_{12}$  clusters for  $n = 1 - 3$ . We observe stable isomers of readily form in  $\text{AuGe}_{12}$  and  $\text{Au}_2\text{Ge}_{12}$ , but not  $\text{Au}_3\text{Ge}_{12}$ . This appears largely due to the nature of the overlap in molecular orbitals at the highest occupied level: it is relatively simple to favor the radially directed Au-Ge bonds in  $n = 1 - 2$  systems, and difficult in  $n = 3$ . We also observe additional stability provided by asymmetric combinations of  $n = 2$  systems and charge in both  $n = 2 - 3$  systems. Our conclusion is that stable Au-Ge clusters or perhaps even extended structures are most likely to be found if 1-2 Au atoms are used to interconnect the equatorial planes of the octahedra, assuming external ligands or large spacing ions were employed to counterbalance ionicity. This suggests that geometry and charge state play a larger role in stable intercluster links than chemical species consistent with Wade's rules.

Remaining still as a theoretical challenge are such problems as is the kinetic nature of Au's role in crystallizing Ge [?] or forming diamond-structure nanowires [?]. Recent work [?] in nanowire growth observes metastable crystalline AuGe catalysts which may further inform which geometries are favored in these nano-sized clusters. Our brief MD studies were not sufficient to make progress in this challenge. But perhaps understanding better Au-Ge bonds in existing compounds should be the center of future studies of this fascinating pair of elements.

## Acknowledgements

This research was supported in part by the assistance and resources of the Notre Dame Center for Research Computing, particularly Paul Brenner and Timothy Stitt.

## 5 Supplementary Material

In Fig. S1 we show the Highest Occupied Molecular Orbital (HOMO) and Lowest Unoccupied Molecular Orbital (LUMO) for the CG-relaxed cluster  $\text{Au}_3\text{Ge}_{18}$ . These figures clearly show the asymmetry of the two  $\text{Ge}_9$  cages. In the LUMO pictures, the right cage shows extended  $\pi$ -like hybridization connecting into triangle of Au atoms. The nodal structure of the orbitals for both cages changes from HOMO to LUMO. Note, COHP for the Au-Au bonds of this cluster is shown in Fig. 8.

In Tables 4 and 6, a number of clusters  $\text{Au}_n\text{Ge}_{12}$ ,  $n = 1, 2, 3$ , are listed and described. Four figures were picked as being representative examples for the main paper and are shown in Fig. 8 (specifically,  $\text{I}_1$ ,  $\text{II}_1$ ,  $\text{I}_2$ , and  $\text{III}_2$ ). The remainder of those clusters are shown in Fig. S2. Clusters  $\text{III}_1$  through  $\text{VII}_1$  are shown only after CG minimization since the isomers have the same overall symmetry and number of bonds as  $\text{I}_1$  and  $\text{II}_1$ , and thus exhibit similar behavior under MD simulation. The rest are shown after both CG minimization and MD simulation.

We show HOMO and LUMO states for five selected CG-relaxed clusters of  $\text{Au}_n\text{Ge}_{12}$ . COHP analysis is also shown for four of these five clusters in Sec. 3.7. In Fig. S3, we show two orientations each for  $\text{AuGe}_{12}$ , cluster  $\text{I}_1$ . Referring back to Fig. 8(a), we see that it is highly symmetric. An interesting feature is the spherical orbital centered on the Au atom, seen in (a) and (c), connecting only loosely to the extended  $\pi$ -like orbitals of the two cages. In the LUMO, (b) and (d), the center Au atom is not directly connected to the cages. As discussed in Sec. 3.7, this cluster is less stable than cluster  $\text{II}_1$ , we show the post-MD rearrangement and symmetry breaking of  $\text{I}_1$  in Fig. 8(a).

In Fig. S4, we show the orbitals after CG minimization for the more stable  $n = 1$  cluster  $\text{II}_1$ . Cluster  $\text{II}_1$  is again highly symmetric [Fig. 8(b)] but interestingly, the HOMO state is degenerate and shows very localized electronic density on the cages, with very minimal interaction with the central Au atom in this orbital. The LUMO state, Fig. S4(c), has electronic structure for the Au bridge site that is similar to that shown in Fig. S3(b), that is, an extended  $\pi$ -like orbital that does not include the central Au atom. The orientations of the cages relative to the bridging Au are different for  $\text{I}_1$  and  $\text{II}_1$ , as seen when comparing Figs. S3 to S4 or comparing the CG picture for  $\text{I}_1$  of Fig. 8(a) to the one for  $\text{II}_1$  in Fig. 8(b).

As Figs. S3 and S4 corresponded to Figs. 8(a) and (b), in Figs. S5 and S6, we show the HOMO and LUMO states for  $n = 2$ , which correspond to the images of CG-relaxed structures in Figs. 8(c) and (d). As discussed in Sec. 3.7, cluster  $\text{I}_2$ , Figs. S5 and 8(c), is more stable than cluster  $\text{III}_2$ , Figs. S6 and 8(d). The cage orbitals for the HOMO state for  $n = 2$  are less extended than for  $n = 1$ . Because of the relative tilting of the two cages for  $\text{I}_2$ , the two Au atoms participate differently in the bonding in the HOMO, Fig. S5. In contrast, for  $\text{III}_2$  shown in Fig. S6, both Au atoms are equally involved in bonding to each other in the HOMO, and not at all in the LUMO.



As seen in Fig. S2, all  $n = 3$  clusters change significantly after a MD run. In Fig. S7, we show HOMO and LUMO for cluster  $\text{I}_3$  to compare these with its CG-relaxed geometry [Fig. S2(h)]. The tilting of the two cages causes two of the three Au atoms to participate differently in the bonding in the HOMO and in the LUMO states. It is most interesting to compare this with the HOMO and LUMO states for  $\text{Au}_3\text{Ge}_{18}$ , Fig. S1. Here we see that the cage electrons in  $\text{Au}_3\text{Ge}_{12}$  are much more localized than in  $\text{Au}_3\text{Ge}_{18}$ .

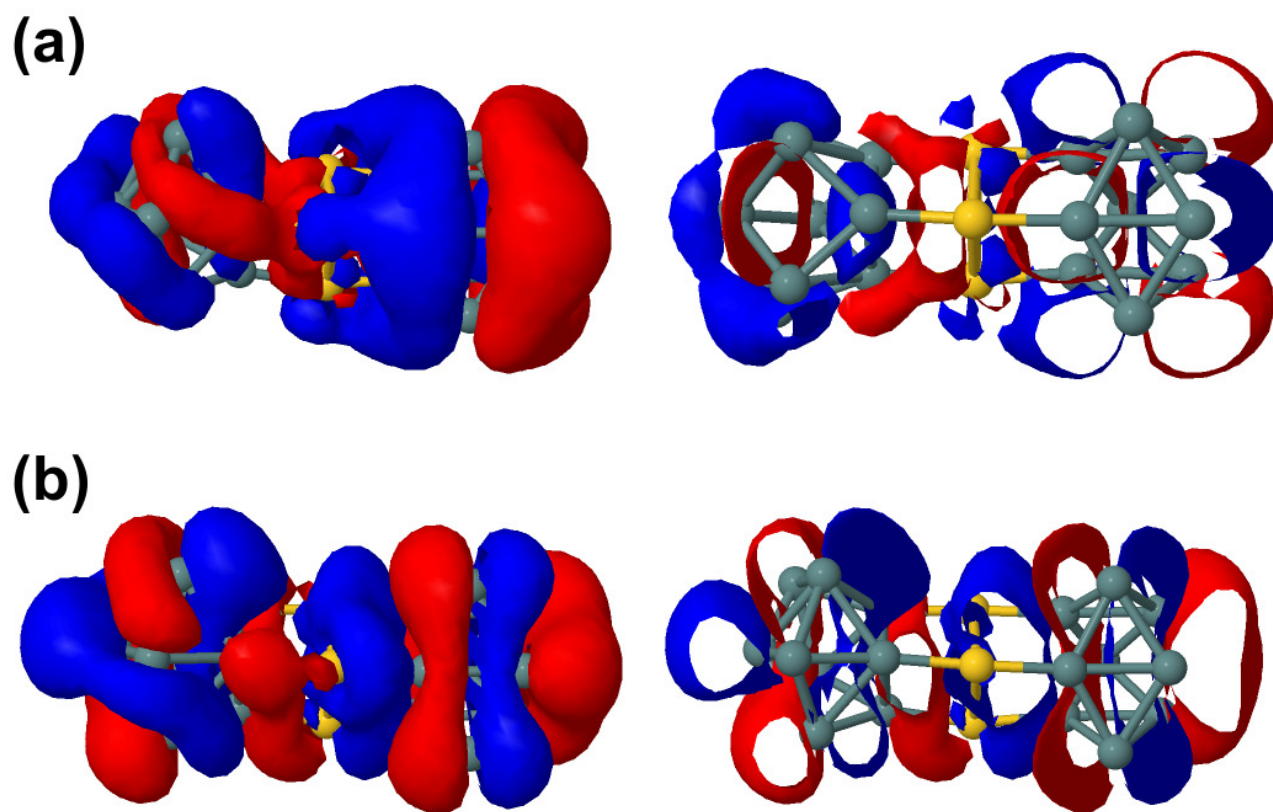


**Fig. S1.** (a) HOMO and (b) LUMO of neutral  $[\text{Au}_3\text{Ge}_{18}]$  where the right column is a slice of the 3D orbitals shown on the left.

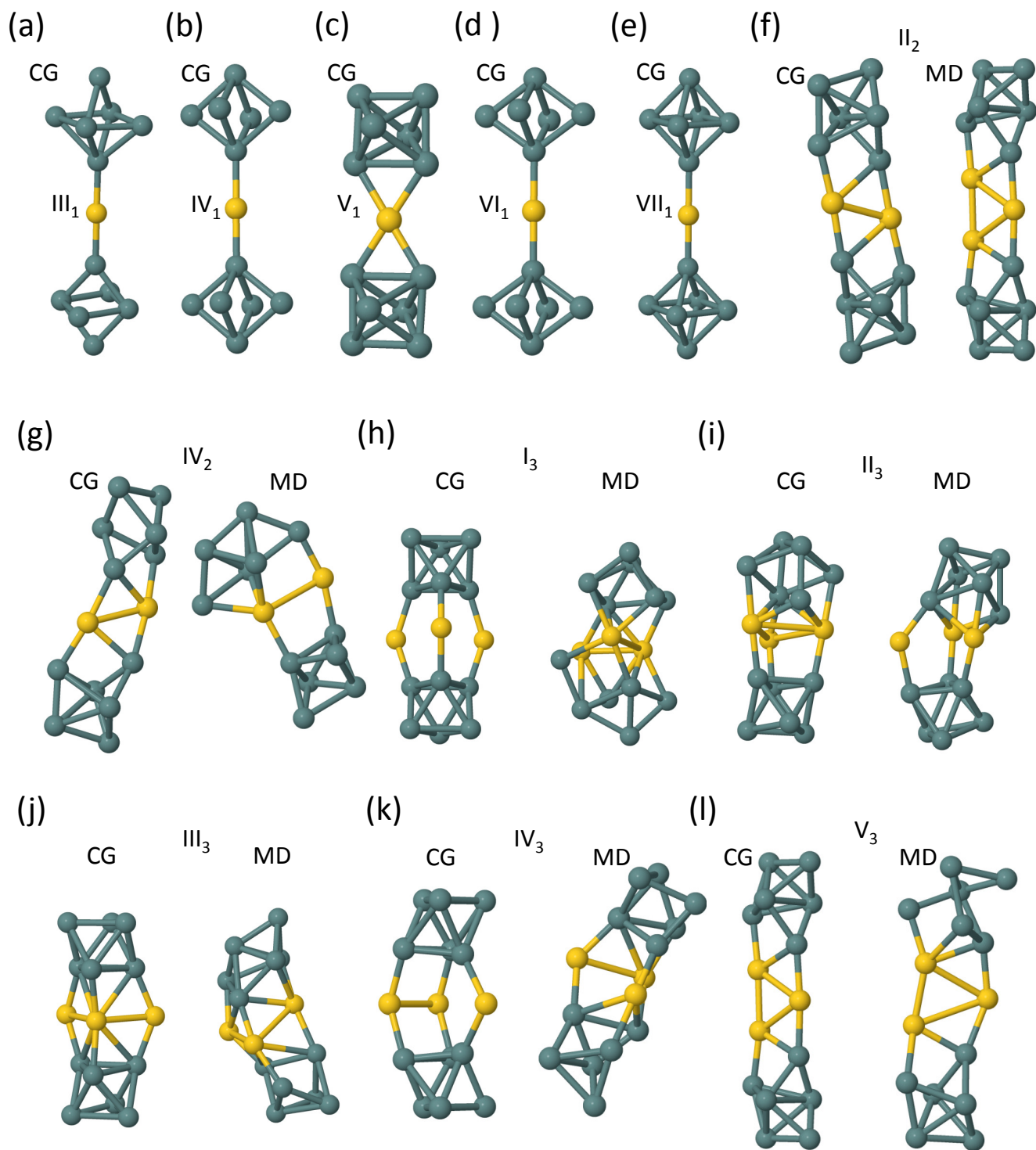


**Fig. S2.** Clusters of  $\text{Au}_n\text{Ge}_{12}$ : (a)-(e),  $n = 1$ ,  $\text{III}_1$ ,  $\text{IV}_1$ ,  $\text{V}_1$ ,  $\text{VI}_1$ ,  $\text{VII}_1$ ; (f) and (g),  $n = 2$ ,  $\text{II}_2$  and (b)  $\text{IV}_2$ ; (h) - (l):  $n = 3$ ,  $\text{I}_3$ ,  $\text{II}_3$ ,  $\text{III}_3$ ,  $\text{IV}_3$ ,  $\text{V}_3$ . For  $n = 1$ , clusters are shown only for after CG minimization. Cluster  $\text{IV}_1$  only differs from  $\text{VI}_1$  due to a smaller horizontal cross section. For  $n = 2, 3$ , clusters are shown after CG minimization and also after a MD run.

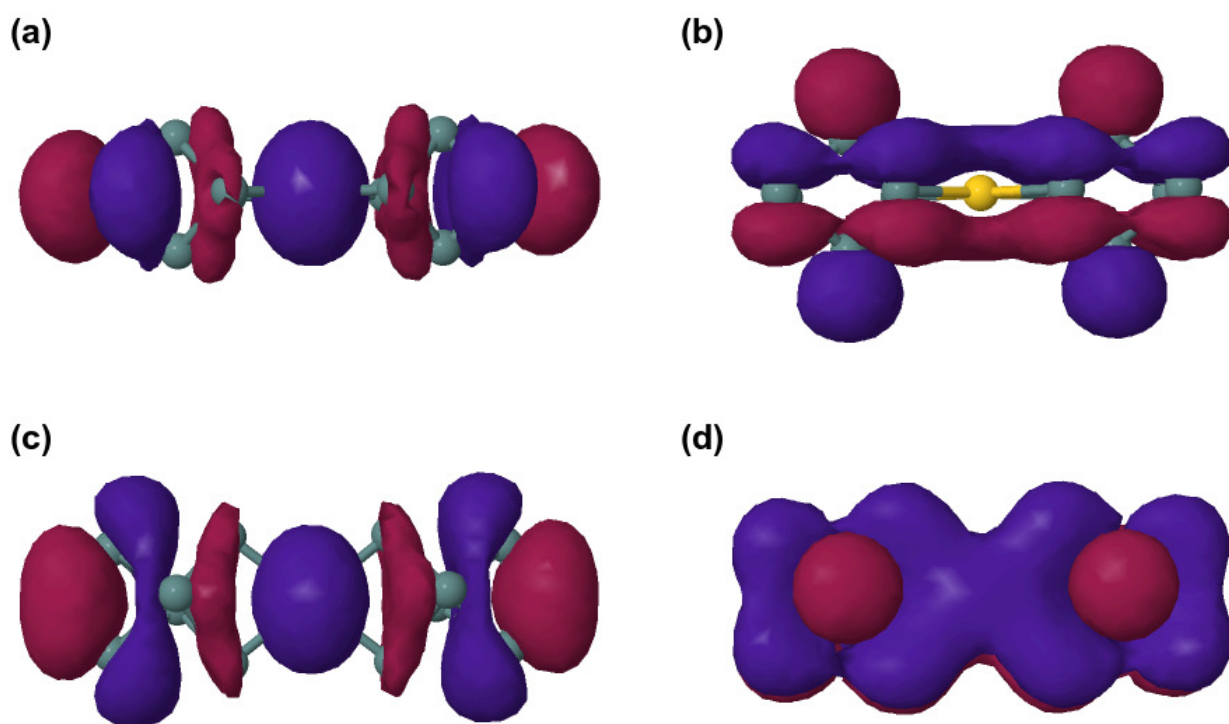


Fig. S3. (a,c) HOMO and (b,d) LUMO of neutral  $\text{AuGe}_{12}$   $I_1$ .

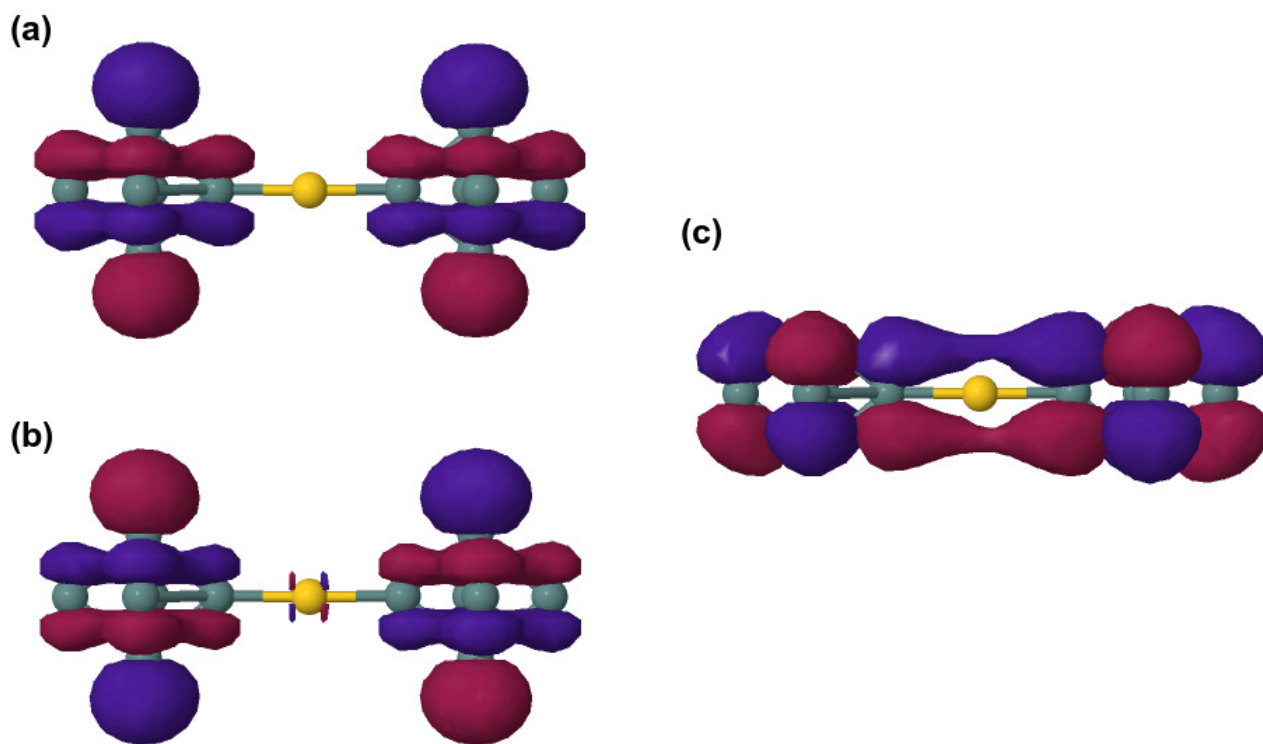


Fig. S4. (a,b) Degenerate HOMO and (c) LUMO of neutral  $\text{AuGe}_{12}$   $II_1$ .

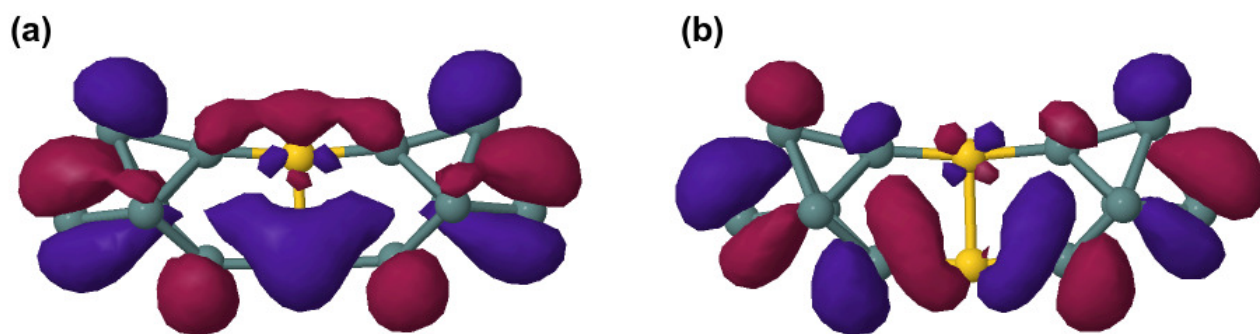


Fig. S5. (a) HOMO states and (b) LUMO of neutral  $\text{Au}_2\text{Ge}_{12} \text{I}_2$ .

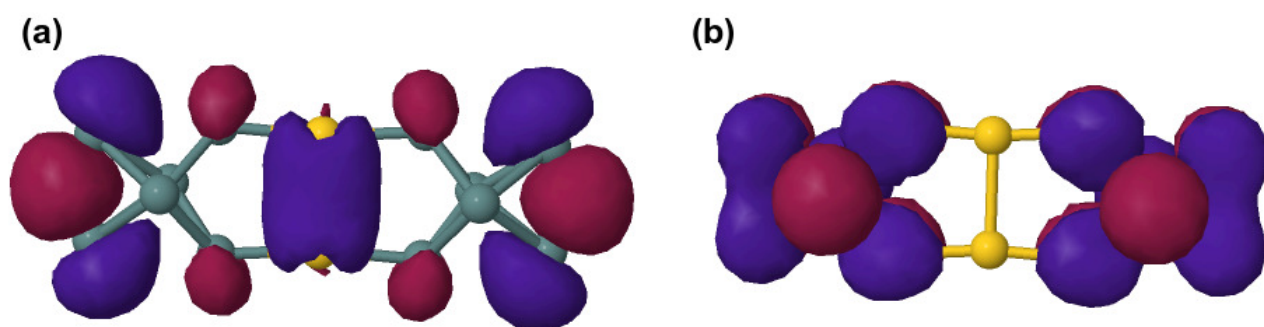


Fig. S6. (a) HOMO and (b) LUMO of neutral  $\text{Au}_2\text{Ge}_{12} \text{III}_2$ .

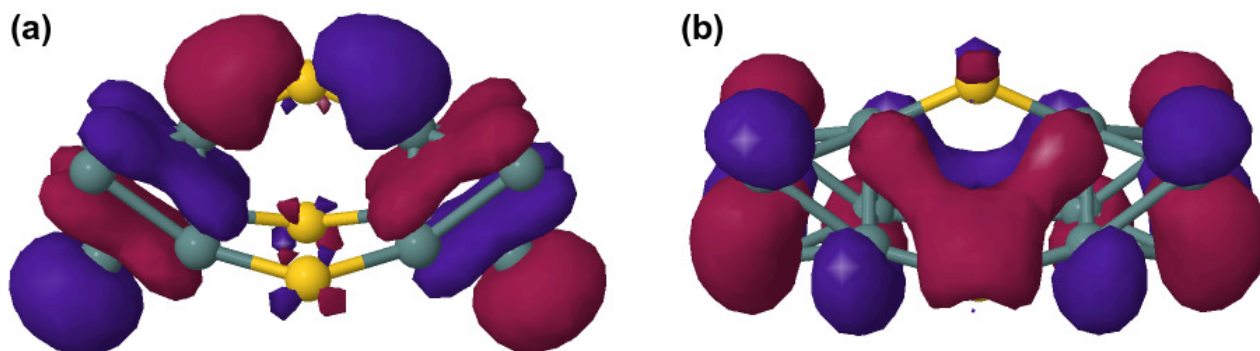


Fig. S7. (a) HOMO and (b) LUMO of neutral  $\text{Au}_3\text{Ge}_{12} \text{I}_3$ .